Efficiency enhancement of a solar dish collector operating with a novel soybean oil-based-MXene nanofluid and different cavity receivers

Navid Aslfattahi [a,*], Reyhaneh Loni [b], Evangelos Bellos [c], Gholamhassan Najafi [b], K. Kadirgama[d], W.S.W. Harun [d], R. Saidur [e,f,*]

[a] Department of Mechanical Engineering, Faculty of Engineering, University of Malaya, 50603, Kuala Lumpur, Malaysia.

[b] Department of Biosystem Engineering, Tarbiat Modares University, Tehran, Iran.

[c] Thermal Department, School of Mechanical Engineering, National Technical University of Athens, Greece.

[d] Faculty of Mechanical and Automotive Engineering Technology, Universiti Malaysia Pahang, Malaysia.

[e] Research Center for Nano-Materials and Energy Technology (RCNMET), School of Science and Technology, Sunway University, Bandar Sunway, Petaling Jaya, 47500, Selangor Darul Ehsan, Malaysia

[f] Department of Engineering, Lancaster University, Lancaster, LA1 4YW, UK

Corresponding authors: Navid Aslfattahi (navid.fth87@yahoo.com) & R. Saidur (saidur@sunway.edu.my)

Abstract

The objective of the present research work is to investigate a novel high-efficiency nanofluid in a solar dish concentrator by using the numerical model developed. The working fluids examined consisted of soybean oil-based MXene nanofluid of different concentrations (i.e. 0.025, 0.075 and 0.125 wt.%) and pure soybean oil. The studied nanofluids yielded excellent thermal properties such as high thermal conductivity and heat capacity, which were two particular factors rendering them excellent candidates for solar thermal applications. The solar dish collector was evaluated for three different cavity receivers including cubical, hemispherical and cylindrical shapes. Then, thermal analysis was performed with a developed numerical model in steady-state conditions, which was validated by using experimental results. Meanwhile, the thermal properties of the oil-based nanofluid were described after the experiments. The analysis was parametric in nature, thereby studying the system performance on a daily basis. According to the analysis, the hemispherical cavity receiver led to maximum thermal efficiency with the nanofluid used. In particular, the daily mean thermal efficiency with nanofluid of 82.66% and the mean equivalent efficiency of 82.46% were achieved,

while the mean enhancement was 0.6%. However, the enhancements were higher with the use of other cavities due to the higher thermal losses shown in such cases. Moreover, the equivalent efficiency proved that the increased pumping work due to the use of nanofluid could not overcome the thermal enhancement, thereby improving the overall performance of the solar collector.

Keywords
Solar dish, novel nanofluid, MXene, efficiency enhancement, parametric study

1. Introduction

Nowadays, the application of solar energy has increased due to the negative impacts of fossil fuel applications, such as global warming, environmental pollution, acid rain and ozone layer depletion. Solar collector works as an efficient heat exchanger for converting solar radiation energy into thermal energy [1, 2]. The solar dish concentrator is underlined as an impactful and high-temperature technology for producing power and heat [3]. Solar dish collector has received great attention amongst various types of solar thermal collectors due to the highest solar to thermal energy conversion efficiency [4, 5]. There are various shapes of receiver for the dish concentrator, consisting of external, cavity, spiral, and volume receivers [6, 7]. Cavity receivers, due to special structure, exhibit higher efficiency in comparison with other types of receivers. Generally, cavity receivers are positioned as a promising component for dish collector systems due to low heat losses [8, 9]. However, enhancement of heat transfer process in the above-mentioned solar energy systems is the most critical issue to boost up the energy efficiency and performance of these compact systems. This issue can be addressed with integration of working fluids with high thermo-physical properties [10]. In contrast, an evaluation of convective heat transfer, and the prediction of Nusselt number in the solar system can be described as important parameters in estimating the thermal performance of the system.

In particular, some research works have been conducted to study the thermal modelling of solar dish concentrators incorporated with cavity receivers [11]. For example, Daabo et al. [12] have investigated the heat flux distribution and optical efficiency of three differently-shaped cavity receivers, namely conical, cylindrical and spherical receivers by using the computational fluid dynamics model and ray-tracing method. The acquired results revealed that the conical shape of the receiver gathered, as well as absorbed, a higher amount of reflected flux energy than the other shapes, with about 91% and 82% for 75% and 85% absorption ratios respectively. Meanwhile, Navalho et al. [13] have investigated the performance of a solar dish collector using a developed model, which is integrated with a volumetric absorber. The authors proved the inability of local thermal equilibrium models and the surface approach for the incoming concentrated solar radiation to accurately predict the receiver hydrothermal performance. Similarly, Bellos et al. [14] have numerically optimized various shapes of cavity receivers as a dish absorber via thermal and optical analyses, thereby identifying the highest optical and thermal performance for the dish concentrator when

using a cylindrical-conical cavity design. According to the acquired results, the worst design is rectangular, while the cylindrical is the fourth design in the performance sequence. Furthermore, Venkatachalam and Cheralathan [15] have considered a solar dish concentrator experimentally by using the various aspect ratios of a conical cavity receiver based on its energy and exergy components. Upon an evaluation of the overall thermal heat losses from the solar dish system, its aspect ratio was found to be an impactful parameter in estimating the thermal performance of the dish collector. The authors proved that the receiver with aspect ratio of 0.8 shown highest performance among all the receivers tested. It is revealed that reduction in receiver surface temperature alone is not adequate to improve the thermal performance, the surface area is also an influencing factor. Besides, Loni et al. [16] have presented a review paper regarding the application of nanofluids as a dominant working fluid of dish concentrators based on experimental tests. Different-shaped cavity receivers as dish absorbers were used, following which they reported the highest thermal performance improvement for the hemispherical cavity receiver with the application of nanofluids. According to the authors, the hemispherical and the cubical cavities are the most effective designs, while the cylindrical cavity presents lower performance. Alternatively, Pavlovic et al. [7] have evaluated a dish concentrator using conical and spiral cavity receivers according to their optical, energy, and exergy components. The authors reported that the conical cavity receiver resulted in better optical and energy performance in comparison with the spiral cavity receiver. The results showed that the conical design leads to a 1.38% increase in the optical efficiency due to the increased intercept factor.

Furthermore, Yan et al. [17] have investigated and optimized a new structure of dish concentrator, whereby the equations for designing the novel dish structure are presented and yield the highest performance. The obtained results showed that the optimized direct solar dish concentrator not only significantly improving the flux uniformity of absorber surface, but also reducing the peak flux and maintaining the excellent optical efficiency between 88.93% and 92.19%. Similarly, Loni et al. [18] have detailed a comparison study related to the energy and exergy performances of a dish concentrator with different shapes of cavity receivers, whereby water and thermal oil are used as the working fluid. They identified the highest exergy performance of the dish concentrator with the application of a hemispherical cavity receiver. Besides, thermal oil and water were introduced as the best options for high-temperature and low-temperature uses, respectively. The authors have used the exergetic efficiency criterion and the overall efficiency criterion in order to evaluate the useful heat production and the pumping power simultaneously. The high exergetic efficiency of the hemispherical cavity with thermal oil at high temperatures makes this case a promising choice for high-temperature solar dish collector applications. Meanwhile, Yang et al. [19] have suggested a new structure for a solar dish concentrator integrated with cavity receiver. The authors reported an enhancement in the optical and thermal performance of the proposed system in comparison with a conventional dish-cavity structure. In another work, several researchers [19] have evaluated the performance of a dish concentrator

numerically and experimentally by using cubical and cylindrical cavity receivers. They realized that the highest thermal performance of the dish collector could be seen when using the cubical cavity receiver in comparison with the cylindrical option. Moreover, Soltani et al. [20] have evaluated the thermal and optical performances of a dish collector with helically-baffled cylindrical cavity receiver. After investigating the different parameters for an optimized performance of the solar system, the authors found that selected optical properties were desirable as effective parameters for increasing the system performance. The authors concluded that the optimal selection of the parameters can enhance the thermal performance of the system up to 65%.

In general, the design of the collectors and the thermophysical properties of the working fluids are commonly considered as the two major factors of solar thermal system, specifically in the aspect of its optical and thermal performance and for the purpose of efficient solar energy harvesting [21]. Nanofluids as the working fluids in the solar thermal system, in particular, play a vital role in generating its enhanced thermal and optical properties due to their superior thermophysical properties [22, 23]. Furthermore, nanofluids have exhibited noticeable enhancements of thermophysical and optical properties over traditional heat transfer fluids [24]. For example, Hong, K. et al. [25] evaluated the thermal and flow characteristics of a parabolic-trough solar collector incorporated with Cu-water nanofluid as heat transfer fluid through numerical analysis. The acquired results proved the significant effect of Cu nanoparticle addition on the heat transfer enhancement while the Reynolds number decreased. This was because nanoparticle addition mainly improved the heat transfer via conduction. According to the authors, as direct normal irradiance increased from 900 to 1100 W m^{-2}, Nu increased by up to 8.6%, 9.78% and 11.43%, respectively, leading to increases in thermal efficiency of 3.87%, 3.82% and 2.04%. Moravej, M. et al. [26] explored the effect of replacing water with surfactant-free rutile TiO_2–water nanofluids as the working fluid in a symmetric flat-plate solar collector. The acquired results showed that the use of TiO_2–water nanofluids can improve thermal efficiency relative to water. The maximum efficiency of the collector, when filled with a 1 wt.% TiO_2-water nanofluid, is found to be approximately 78%; this represents maximum and average efficiency gains of 9.80% and 6.64%, respectively, relative to the water baseline. Bozorg, M.V. et al. [27] investigated the performance of a novel parabolic trough solar collector with synthetic oil–Al_2O_3 nanofluid as the heat transfer fluid through finite volume method. The acquired results show that as Reynolds number and volume fraction of nanoparticle increase, heat transfer coefficient, pressure drop, and thermal efficiency increase. However, the increases in inlet temperature lead to the decreases in heat transfer coefficient, pressure drop, and thermal efficiency. Khan et al. [28] have investigated the overall energy efficiency of a parabolic dish solar collector integrated with a cavity receiver and thermal oil-based nanofluids incorporating various types of nanoparticles, including Al_2O_3, CuO, and TiO_2. The authors reported the highest overall energy efficiency of 33.73% for the Al_2O_3-based nanofluid. Meanwhile, another research work has investigated the efficiency of the solar dish collector by using base fluid and Al_2O_3-based nanofluid under various operating conditions. As a result,

the researchers reported a higher efficiency of 10% for the solar dish collector integrated with nanofluid (i.e. inclusion of 0.01 volume concentration) in comparison with the collectors integrated with base fluid as working fluid. Similarly, Pavlovic et al. [29] have conducted an experimental work using Syltherm 800 oil as the base fluid and Cu/TiO_2 nanoparticles as the additives in the synthesis of mono and hybrid nanofluids. This was done as a comparison study for the investigation of performance enhancement in a solar dish collector. Subsequently, the researchers reported better thermal efficiency performance for the solar dish collector when using hybrid nanofluid (i.e. 0.99% mean enhancement compared to base fluid) as opposed to the mono nanofluid. Alternatively, Rajendran et al. [30] have investigated the energy efficiency of a cavity receiver integrated with a solar dish collector, which works with the base fluid and SiC-water nanofluid. According to the authors, an enhancement of 12.94% was observed in the energy efficiency for the solar dish collector working with nanofluid in comparison with the base fluid. In similar approach, Loni et al. [31] have investigated various nanofluids in a solar dish collector integrated with spiral cavity absorber according to their thermal and exergy analyses, thus reporting the high exergy and thermal efficiencies of 35% and 10%, respectively. In another study, the effect of various nanofluids on the exergetic performance of a solar dish collector integrated with smooth and corrugated spiral absorbers has been investigated [32]. Accordingly, the authors yielded better exergetic efficiency for oil-based nanofluids, while water-based nanofluids generated better thermal efficiency. In another study, Loni et al. [33] have evaluated the effect of MWCNT/oil-based nanofluid on the thermal performance of a hemispherical cavity receiver in a solar dish collector system. As a result, the authors reported a prominent enhancement of 13% in the thermal performance of the collector examined.

MXenes are an emerging two-dimensional layered nanomaterial first discovered by Drexel University in 2011 [34]. Due to the superior properties of this novel nanomaterial, numerous theoretical and/or experimental studies have been carried out accordingly [35]. The MXene family materials are recognized for their prominent thermal, optical, electrical, and other promising properties. These unique nanomaterials are defined using a general formula of $M_{n+1} X_n T_x$ (n=1-3), where M stands for early transition metals (Ti, V, Sc, Ta, Cr, Mo, Zr, Hf, Nb), X indicates the C and/or N atoms, and T_x illustrates the surface termination groups (-O, -OH, and -F). MXenes are mostly synthesized through the selective etching of A-element layers from their precursor MAX phase parent materials with the hydrofluoric acid (HF)/in-situ preparation of HF etchants. Due to prominent metallic conductivity, hydrophilic surface, and excellent mechanical properties, MXenes family materials have gained extensive attention from researchers for their applicability in various potential products. This includes super-capacitors, lithium/non-lithium ion batteries, and as reinforcement in polymers and solar systems [36, 37]. Li et al. [38] have proven that the light-to-heat conversion efficiency of MXene (Ti_3C_2) is almost 100%. This reveals an excellent energy conversion potential for the novel nanomaterial and a further proof of their applicability in solar energy harvesting systems. Furthermore, Fu et al. [39] have fabricated MXene-

contacted silicon solar cells with an overall power conversion efficiency of 11.5% to demonstrate the remarkable potential of MXene composites as the electrodes for developing highly efficient solar cells. In another study, some researchers have reported 12% enhancement in the efficient performance of solar system due to the presence of 0.03 wt.% MXene [40].

In this research work, a novel nanofluid with MXene and soybean oil is investigated experimentally and numerically in a solar dish collector for the first time. Therefore, the thermal conductivity, density, specific heat capacity, and dynamic viscosity of the developed nanofluid are evaluated experimentally first and then used as the input parameters for the subsequent numerical analysis. The developed nanofluid revealed promising enhancement of almost 24.49% in the specific heat capacity due to the presence of novel MXene nanoparticles. In this regard, such investigation of energy performance and pumping work of the solar dish collector integrated with various cavity receivers by using the newly-formulated soybean oil-based nanofluid is the first study, to the best of the authors' knowledge. Besides, the overall efficiency analysis as a function of inlet temperature for the three different nanoparticle concentrations of the developed nanofluid is another new finding from this research work, as well as the base fluid in various cavity receivers (i.e. hemispherical, cylindrical, and cubical-shaped). Therefore, the thermal efficiency analysis conducted for the three different cavity receivers by using the developed nanofluid inclusive of the inlet temperature variation generated the best performance when the hemispherical shape cavity receiver was utilized. Meanwhile, the highest concentration of developed nanofluid was noted as the best candidate for parametric analysis. Hence, the parametric performance of the hemispherical cavity receiver with nanofluid of 0.125 wt.% concentration and pure oil was examined at different volumetric flow rates (5-150 ml/s) and solar beam irradiation levels (600-900 W/m^2). Moreover, the daily performance analysis of the system for the hemispherical cavity receiver with nanofluid containing a concentration of 0.125 wt.% (optimized features based on the comprehensive analysis) was another interesting outcome obtained. The daily mean thermal efficiency with nanofluid was recorded as 82.66% and the mean equivalent efficiency was 82.46%. Therefore, the current research work highlighted the energy conversion efficiency of the developed nanofluid following the presence of MXene nanomaterials. This was achieved through different cavity receivers integrated with a solar dish collector as an efficient heat exchanger for converting the solar irradiation into efficient thermal energy as clean source of energy. Findings of this research work gives strong justification for using the newly developed nanofluid for improvement of energy conversion and energy efficiency in solar dish collector integrated with various types of cavity receivers.

2. Material and Methods

In this section, the methodology employed to investigate the performance of a solar dish collector integrated with three different shapes of cavity receiver is presented. It should be noted that the application of MXene/vegetable oil nanofluid as the working fluid for the solar system was investigated accordingly. All of the acquired thermophysical properties were experimentally calculated at different temperatures and volume fractions based on some experimental tests. A summary of the methodology can be presented as follows:

- Thermal and optical modelling of a solar dish collector integrated with various shapes of cavity receivers, including hemispherical, cubical, and cylindrical, were conducted.
- The thermophysical properties of a new nanofluid, namely MXene/vegetable oil nanofluid, were experimentally calculated at different temperatures.
- The thermal performance of the solar system with various cavity receivers was investigated based on the application of the MXene/vegetable oil nanofluid as the working fluid and under variety of inlet temperatures and volume fractions.
- The solar dish collector integrated with hemispherical-shaped cavity receiver was evaluated using a parametric study. The impact of solar radiation and nanofluid's volume flow rate was investigated accordingly. Moreover, the daily performance of the solar system with MXene/vegetable oil nanofluid as working fluid was numerically investigated based on real conditions.
- Finally, the validation of the developed model performed based on the experimental data reported.

2.1. Optical and Thermal Modelling

In this research work, the internal heat transfer of three differently-shaped cavity receivers was investigated on the basis of numerical method. A solar dish concentrator integrated with various tubular cavity receivers was evaluated via optical and thermal analyses. Three different shapes of cavity receiver, namely cubical, cylindrical and hemispherical were considered. It should be mentioned that the real optical and structural parameters of a dish concentrator integrated with tubular cavity receivers were used, such as solar dish reflectivity of 0.84, tracking error of 1º, optical error of 10 mrad, dish aperture diameter of 1.9 m, focal dish distance of 0.693 m, cubical aperture width and height of 14 cm, cylindrical aperture diameter and height of 12.5 cm, cavity tube diameter of 10 mm and aperture hemispherical diameter of 12 cm [41]. Meanwhile, the dimensions of the cavity receiver were adopted based on the optimization analyses conducted previously by Loni et al. [3], [6], [42], specifically for the cubical, cylindrical, and hemispherical cavity receivers, respectively. In addition, it should be noted that the optimized cavity receivers as mentioned above were built and tested using oil and different oil-based nanofluids such as alumina/oil, silica/oil, and CNT/oil nanofluids based on experimental tests by different authors [11, 43-45]. Figure 1. illustrates a schematic of the investigated solar system integrated with various cavity receivers.

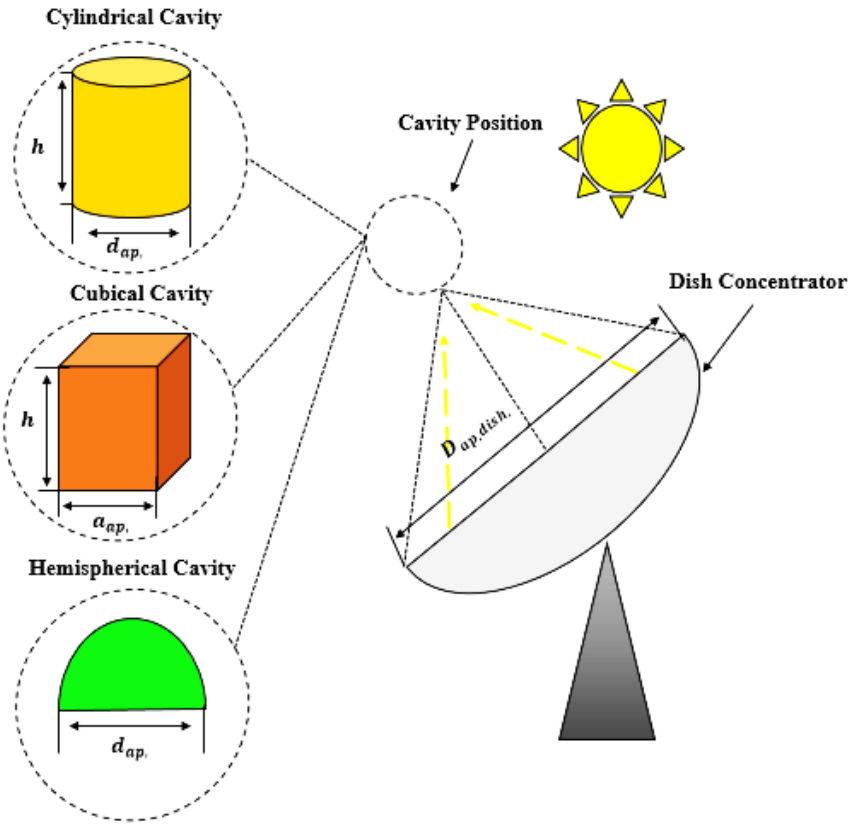

Figure 1: A schematic of the investigated solar system with different cavity receivers.

Analyses for the current study were conducted in two steps. In the first step, the optical performance of the solar system was evaluated by implementing the SolTrace software, whereby estimations of the heat flux distribution along the cavity tubes and absorbed solar heat flux by the cavity walls were generated. A view of the optical analysis for the dish concentrator using the three tubular cavity receivers investigated is presented in Figure 2. In the second step, the thermal performance of the solar systems was numerically developed in the Maple software, followed by using the energy balance equations and thermal resistance methods for thermal modelling. Meanwhile, the internal heat transfer of the working fluid was numerically developed and investigated in the tubular cavity receivers accordingly.

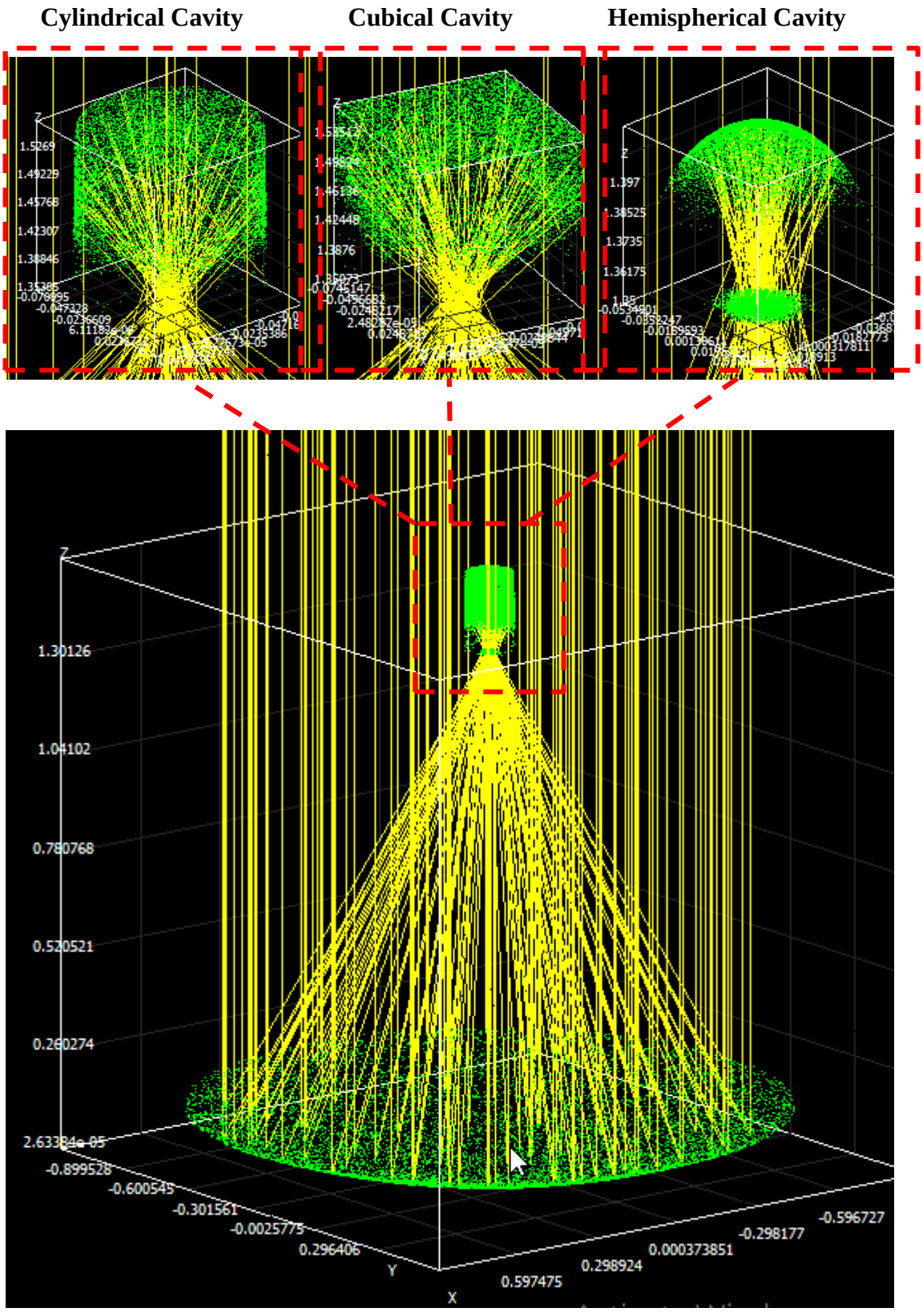

Figure 2: A view of the optical analysis for the dish concentrator using with three tubular cavity receivers.

In this section, the thermal modelling developed for the solar focal point concentrator is presented. As mentioned earlier, the thermal modeling of the solar system is conducted using the energy balance equations. Generally, heat losses from the cavity receivers consisted of convection, conduction, and radiation-based losses. It should be mentioned that the cavity receivers were insulated with mineral wool to reduce losses. Therefore, the conduction heat losses were accrued from the insulation layer of 5 cm thickness, whereas the convection heat losses occurred from the inside of the cavity receivers and outside of the wall cavity receivers. Finally, radiation heat losses from the inner space of the cavity receivers were underlined during thermal modelling. Table 1. represents the main evaluated parameters of the studied solar dish collector in the simulation process.

Table 1: The main parameters of the solar dish collector examined in the simulation.

Parameter	Value
Dish diameter	1.8m
Focal distance	1.35m
Collecting area	2.545m^2
Outer tube diameter	10mm
Inner tube diameter	9mm
Emittance of the absorbing area	0.10
Absorbance of the cavity	0.84
Concentrator reflectance	0.90
Cavity inner diameter	140mm
Cavity outer diameter	160mm
Cavity height	140mm
Coils in cubical cavity	12
Coils in cylindrical cavity	14
Coils in hemispherical cavity	10

Absorbed heat by the working fluid ($\dot{Q}_u$) can be calculated as follows [46]:

$$\dot{Q}_u = \dot{Q}^* - \dot{Q}_{loss} \quad (1)$$

Where $\dot{Q}^*$(W) is the rate of available solar heat received by the cavity walls that can be calculated using SolTrace and $\dot{Q}_{loss}$(W) is the heat losses from the cavity receiver that can be estimated using the equation below [46]:

$$\dot{Q}_{loss} = \dot{Q}_{loss,cond} + \dot{Q}_{loss,rad} + \dot{Q}_{loss,conv} \quad (2)$$

Where $\dot{Q}_{loss,cond}$(W) is the conduction heat losses, $\dot{Q}_{loss,rad}$(W) is the radiation heat losses, and $\dot{Q}_{loss,conv}$(W) is the convection heat losses. More details about the heat loss calculation from the cubical, cylindrical, and hemispherical cavity receivers are

presented in references [3], [6], and [42], respectively. It should be noted that following equation is used for the calculation of the thermal efficiency of the solar system [46]:

$$\eta_{th} = \frac{\dot{Q}_u}{\dot{Q}_{solar}} \tag{3}$$

Where $\dot{Q}_{solar}$(W) is the received solar energy by the dish concentrator that can be calculated as shown below [46]:

$$\dot{Q}_{solar} = I_b \cdot \frac{\pi \cdot D_{ap,dish}^2}{4} \tag{4}$$

In this equation, I_b (W/m^2) is the solar direct beam radiation and $D_{ap,dish}$ (m) is the aperture dish diameter. The cavity tube was divided into smaller elements along the receiver tube of the three cavity receivers to ensure more accuracy in the calculated results. Then, the receiver surface temperature ($T_{s,n}$) and useful heat flow ($\dot{Q}_{u,n}$) at different elements of the tube are calculated by solving the equations detailed in this subsection via the Newton–Raphson Method [46]:

$$\dot{Q}_{u,n} = \frac{(T_{s,n} - \sum_{i=1}^{n-1}\left(\frac{\dot{Q}_{u,i}}{\dot{m} \cdot c_{p0}}\right) - T_{in,0})}{(\frac{1}{h_{inner} \cdot A_n} + \frac{1}{2 \cdot \dot{m} \cdot c_{p0}})} \tag{5}$$

In this equation, $\dot{m}$ is the system mass flow rate, c_{p0} is the constant pressure specific heat and A_n is the area.

The Nusselt number of the internal working fluid flow (Nu_{inner}) is estimated as [47]:

$$Nu_{inner} = \frac{\left(\frac{f_r}{8}\right) \cdot Re \cdot Pr}{1 + 12.8 \cdot \sqrt{\frac{f_r}{8}} . (Pr^{0.68} - 1)} \tag{6}$$

The friction factor (f_r) is calculated as [47]:

$$f_r = (0.79 \cdot \ln Re - 1.64)^{-2} \tag{7}$$

In addition, the inner heat transfer coefficient (h_{inner}) is calculated as [48]:

$$h_{inner} = \frac{Nu_{inner} \cdot k_{fluid}}{d_{tube}} \tag{8}$$

In this equation, k_{fluid} shows the thermal conductivity of working fluid.

The net heat transfer rate can be calculated using the equations below [46]:

$$\dot{Q}_{u,n} = \dot{Q}^*_n - \dot{Q}_{loss,rad,n} - \dot{Q}_{loss,internal\ conv,n} - \dot{Q}_{loss,external\ conv,n} \quad (9)$$

$$\dot{Q}_{u,n} = \dot{Q}^*_n - A_n \cdot \varepsilon_n \cdot \sigma \cdot \left(T_{s,n}{}^4\right) + A_n \sum_{j=1}^{N} F_{n-j} \cdot \varepsilon_j \cdot \sigma \cdot \left(T_{s,n}{}^4\right) - A_n \cdot \varepsilon_n.\sigma \cdot F_{n-\infty} \cdot T_\infty^4 - A_n \cdot \left(m_2 \cdot T_{s,n} + c_2\right) - \frac{A_n}{R_{cond}}\left(T_{s,n} - T_\infty\right) \quad (10)$$

The pressure drop (ΔP) is calculated as shown below:

$$\Delta P = f_r \cdot \frac{L}{d_{tube}} \cdot \left(\frac{1}{2} \cdot \rho \cdot u^2\right) \quad (11)$$

The pumping work demand (W) is calculated as:

$$W = \frac{\dot{m} \cdot \Delta P}{\rho} \quad (12)$$

The overall efficiency (η_{ovr}) states the net efficiency of the systems and takes into consideration of the pumping work demand and the useful heat production (Q_u). In practice, the pumping work is converted into an equivalent primary heat through the conversion efficiency (η_{conv}), which can be assumed as equivalent to 33% [49].

$$\eta_{ovr} = \frac{Q_u - \frac{W}{\eta_{conv}}}{Q_{solar}} \quad (13)$$

2.2. Thermophysical properties of developed nanofluids

The aforementioned two-step method was utilised accordingly for the formulation of soybean oil-based Ti_3C_2 nanofluid. Three different loading concentrations of MXene were loaded into the base fluid, namely 0.025, 0.075, and 0.125 wt.%. Afterwards, the stirring process was conducted for 30 min using a hot plate magnet stirrer (RCT basic IKAMAG® safety control) at 700 rpm and temperature of 70 °C for the acquisition of a homogenous mixture. The suspensions of Ti_3C_2 and soybean oil were then sonicated (1200W, 20kHz) for 30 min using an ultrasonic probe sonicator (FS-1200N), which would agitate the intermolecular forces between the Ti_3C_2 nanomaterials and cause them to disperse uniformly. The final product revealed a well-dispersed nanofluid due to the advantageous feature of the probe sonicator, which separated the cluster of nanoparticles inside the base fluid. Detailed information regarding the developed nanofluids and experimental measurements is elaborated extensively in our previous research study [50].

2.2.1 Density analysis

A temperature-dependent density measurement was conducted using a densitometer (Anton Paar, Density Meter, Model: DMA™1001). An accurate calibration of the densitometer was first performed by using air and pure distilled water. Then, the sample density was measured as a function of temperature from 25 °C to 55

°C with repeatability of 0.00005 g/cm³ and accuracy of 0.0001 g/cm³. Figure 3 demonstrates the experimental results acquired for density analysis.

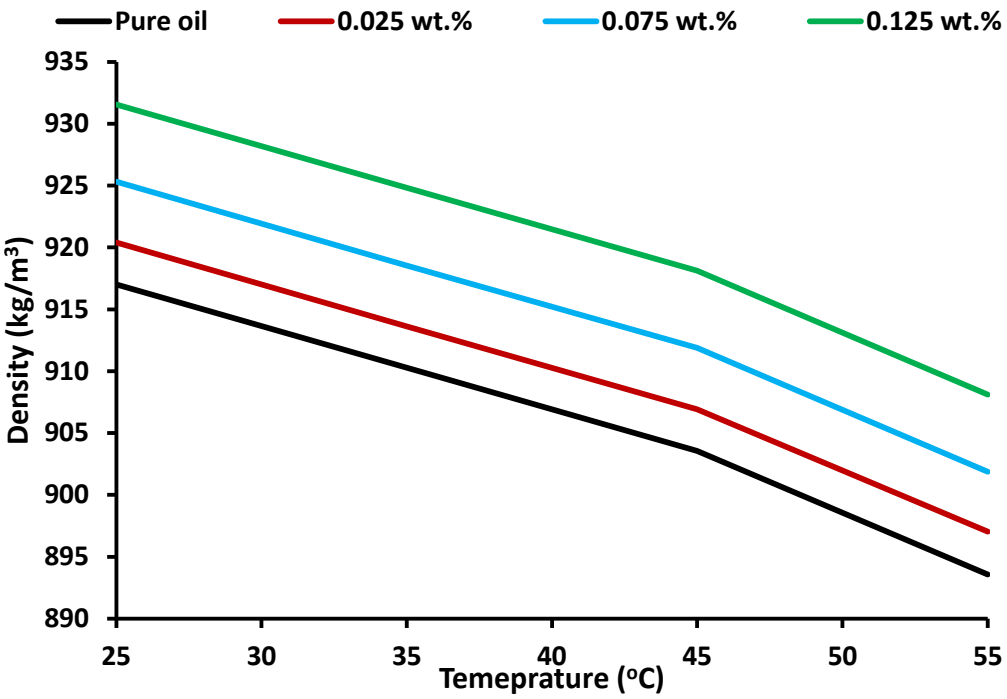

Figure 3: Density of the examined fluids.

2.2.2 Specific heat capacity measurements

In this study, Differential Scanning Calorimetry (DSC) DSC-1000/C (Linseis, Germany) was employed for the specific heat capacity measurements. The instrument conducted high-resolution (0.03 µW) measurements, whereby the samples were placed in a 40 µl aluminium crucible. Then, they were heated at 10°C/min to achieve the results in the temperature range of 25-55 °C. Figure 4 presents the experimental results for the specific heat capacity measurements, which are conducted under nitrogen atmosphere with a fixed flow rate of 20 ml/min.

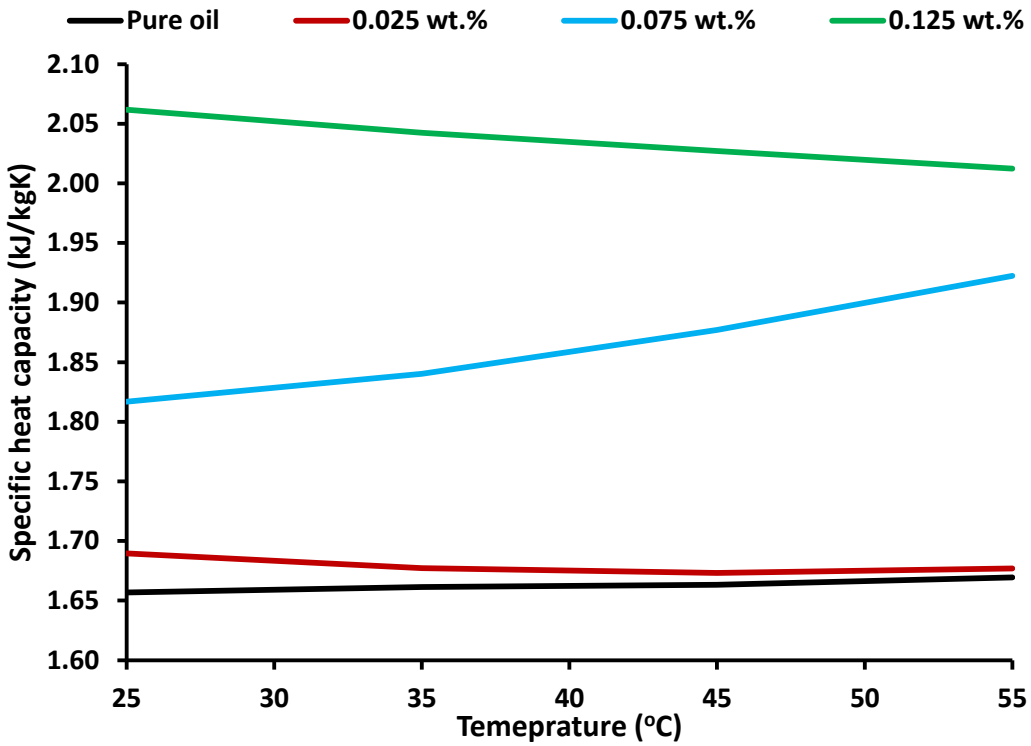

Figure 1: Specific heat capacity of the examined fluids.

2.2.3 Thermal conductivity analysis

Figure 5 illustrates the thermal conductivity measurements conducted for the nanofluid developed. The thermal conductivity analysis for the soybean oil and soybean oil-based Ti_3C_2 nanofluids was performed using a thermal properties analyzer (Tempos meter). Sensor KS-3 (1.3 mm diameter × 60 mm length) was employed to conduct the experiments as it was particularly positioned for low thermal conductivity measurements (thermal conductivity: 0.02–2.00 W/mK). In particular, Tempos functioned by using hot-wire technique with a maximum error of less than ±10%. Each measurement was repeated five times to achieve precise data, whereby the resulting mean value was used in the numerical study.

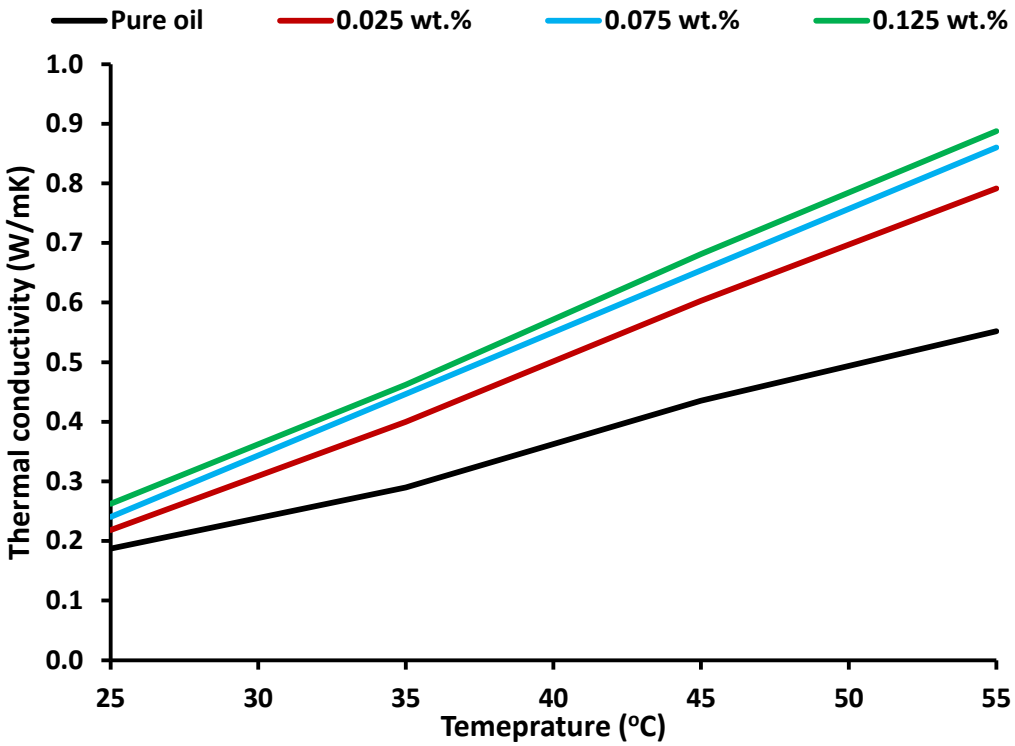

Figure 5: Thermal conductivity of the examined fluids.

2.2.4 Dynamic viscosity measurement

Dynamic viscosity of the developed nanofluid as a function of temperature was measured using the MCR 92 Rheometer (Anton Paar), where its precision was ±1.0% (from -40 to 200°C). Calibration of the equipment was performed by using pure distilled water for accuracy purposes in which a spindle (Meas. Cylinder B-DG42) was used for the measurement. Figure 6 presents the experimental data acquired for the dynamic viscosity of developed nanofluid as a function of temperature.

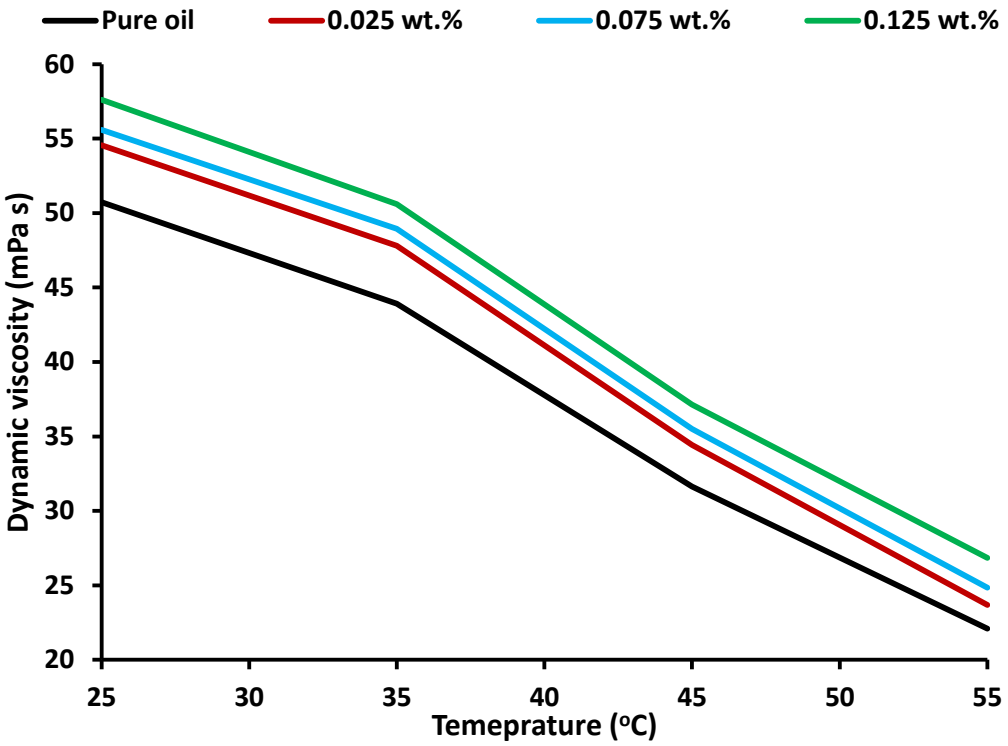

Figure 6: Dynamic viscosity of the examined fluids.

2.3. Validation evidence of the developed model

The numerical results of this study were validated based on specific experimental results obtained in the Renewable Energy Research carried out at Tarbiat Modares University, Tehran, Iran (located at 35.68° N latitude and 51.42° longitude). The experimental setup consisted of a dish concentrator, hemispherical cavity receiver, and hydraulic cycle (see Figure 7). Working fluid for this system was thermal oil. Similarly, the inlet and outlet temperatures of the working fluid at the inlet and outlet of the cavity receiver were measured during the experimental tests, as well as the working fluid volume flow rate. Meanwhile, the ambient parameters such as ambient temperature, solar radiation and wind speed were measured as well. More details related to the experimental tests are as reported by reference [44]. The mean deviation was 3.04%, which was a relatively low value; thus, the model was accepted as reliable. It should be noted that higher deviations far from the solar noon could be observed due to higher tracking errors of the experimental setup at the respective solar positions (see Table 2).

Figure 7: The solar dish collector examined [44].

Table 2: Validation of the model developed with experimental results [44].

Time	T_{in}	T_{out}	I_b	T_{amb}	V_{wind}	V	Experiment		Model		Deviation
							Q_u	η_{th}	Q_u	η_{th}	
(h)	(˚C)	(˚C)	(W/m^2)	(˚C)	(m/s)	(ml/s)	(W)	(%)	(W)	(%)	(%)
9:30	41.1	118.1	752.8	26.9	1.2	10	1335	62.6	1533	68.0	8.63
10:00	40.0	120.4	774.3	27.8	0.5	10	1395	63.6	1579	68.4	7.55
10:30	51.2	135.9	790.8	28.0	1.3	10	1479	66.0	1604	68.0	3.03
11:00	46.4	133.8	805.0	29.0	0.8	10	1530	67.1	1636	68.1	1.49
11:15	47.4	137.1	824.2	29.0	1.2	10	1567	67.1	1673	68.0	1.34
11:45	43.8	137.3	849.0	31.3	1.0	10	1638	68.1	1724	68.1	0.00
12:30	42.3	137.8	859.2	31.6	1.6	10	1656	68.0	1744	68.0	0.00
13:00	43.2	135.4	841.6	31.5	1.4	10	1615	67.7	1709	68.1	0.59
13:30	46.1	136.7	833.5	31.0	0.5	10	1591	67.4	1694	68.1	1.04
13:45	47.9	135.7	810.6	31.0	2.1	10	1542	67.1	1644	68.0	1.34
14:00	56.0	134.3	774.6	30.0	0.6	10	1376	62.7	1571	68.0	8.45

3. Results and discussion

This section is devoted to presenting the results of the simulation carried out, specifically regarding the performance generated by different cavity receivers with the nanofluid. Comparison with the conducted operations is performed with an alternative material, namely pure oil. Accordingly, parametric studies are processed to yield the different values of volumetric flow rate, inlet temperature and solar irradiation. The

thermal efficiency and overall efficiency make up the evaluation criteria implemented in the process.

3.1 Comparison of cavity receivers

Section 3.1 includes the results obtained from the operation using the three cavity receivers examined, as well as the comparative results generated to determine the most effective cavity and the most promising working fluid accordingly.

3.1.1 Analysis with the cubical receiver

The first receiver examined was the cubical cavity receiver. Figure 8 shows that thermal efficiency reduces the inlet temperature increment, which is a reasonable outcome. A higher inlet temperature led to higher thermal losses and consequently resulted in lower thermal efficiency. Moreover, the use of nanofluids yielded higher thermal efficiency compared to the operation with pure oil. In addition, it is important to state that higher nanofluid concentrations would lead to higher thermal efficiency. This result indicates that when higher amounts of nanofluids are used, a greater potential can be perceived for improving the collector efficiency. Figure 9, demonstrates the thermal efficiency enhancement values for the nanofluids examined. It could be said that the enhancement is mainly dependent on the nanoparticle concentration rather than the operating temperature level. The enhancement with the 0.025 wt.% concentration was around 1.7%, while it was 2.2% for 0.075 wt.% and 2.4% for 0.125 wt.% concentrations.

However, the use of nanofluids was associated with the increased dynamic viscosity, which increased the pressure drop and consequently the pumping work demand for the fluid circulation. Figure 10, illustrates that the nanofluids lead to higher pumping work for all examined temperatures. To properly evaluation of the pumping work increase, the criterion of the overall efficiency was used and revealed the collector efficiency in terms of the net useful heat production. In practice, the pumping work demand was converted into equivalent heat by diving it with 0.33 (typical value), which was then reduced by the useful heat production. This criterion shows that the use of nanofluids leads to higher performance in comparison with the pure oil case, as Figure 11 indicates. This result is very important because it proves that the increased pumping work with nanofluid is unable to overcome the thermal efficiency enhancement. Therefore, this criterion proved that the higher-pressure drop limitation could be faced properly. It must be noted that according to the overall efficiency, the best concentration was 0.125 wt.% for temperatures ranging from 35°C to 50°C, while at 55°C, both concentrations (i.e. 0.125 and 0.075 wt.%) yielded similar values.

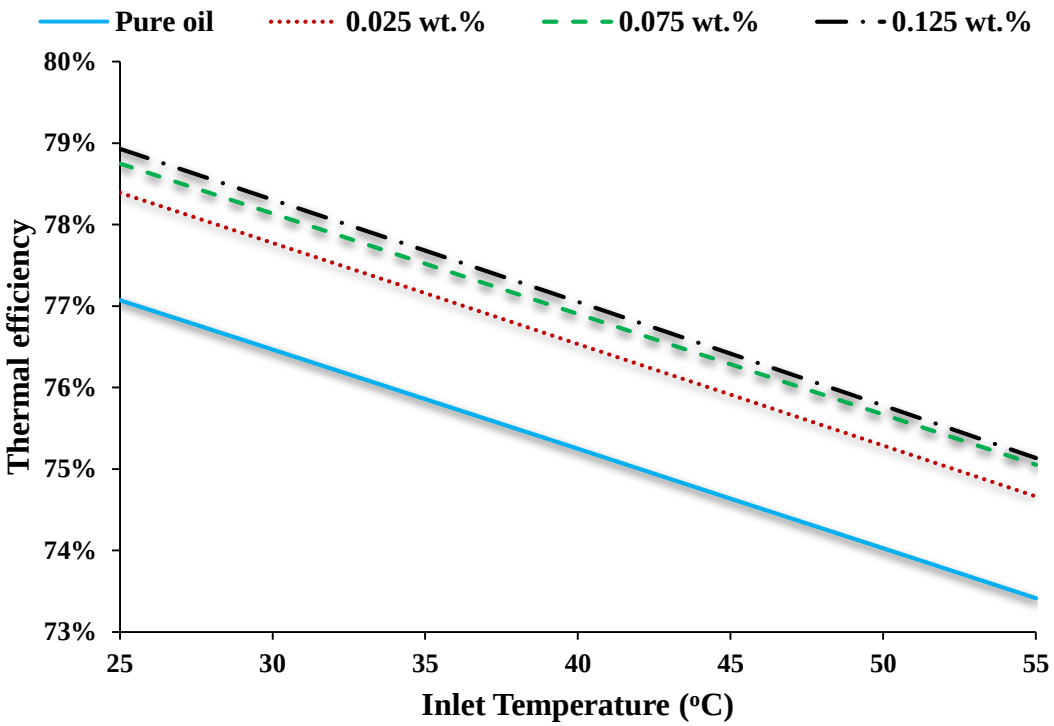

Figure 8. Thermal efficiency of the cubical receiver for different inlet temperatures for the examined working fluids.

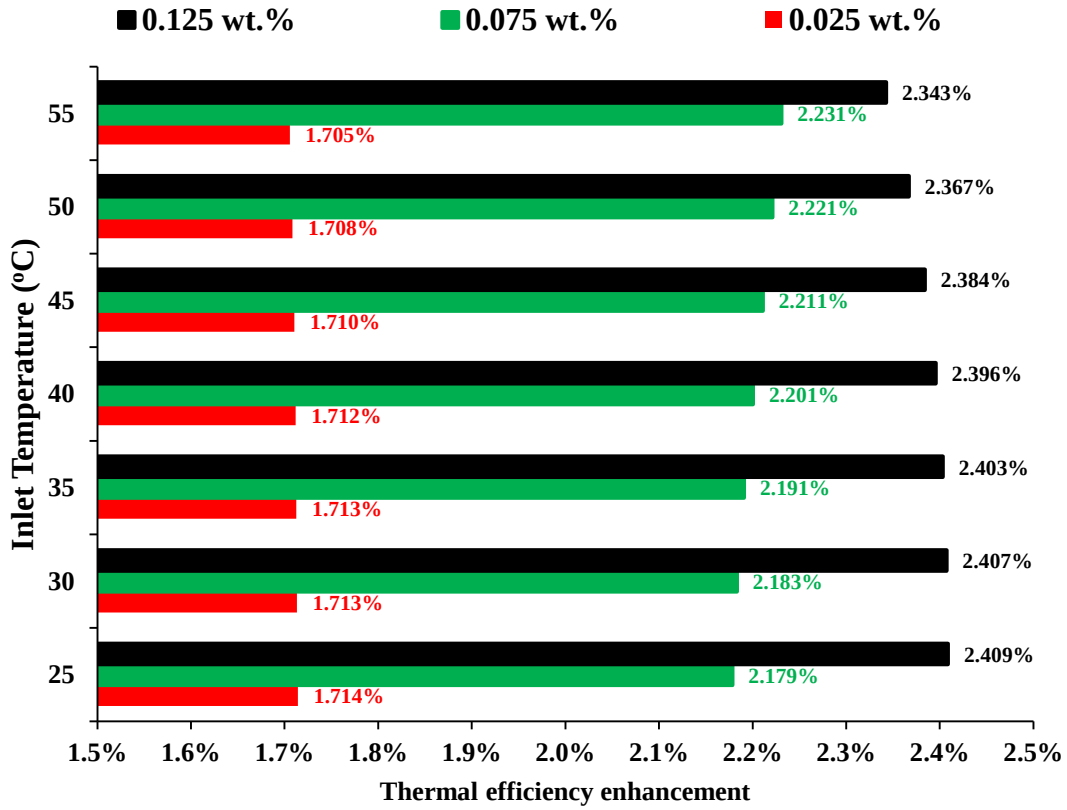

Figure 9. Thermal efficiency enhancement of the cubical receiver for different inlet temperatures for the examined nanofluids.

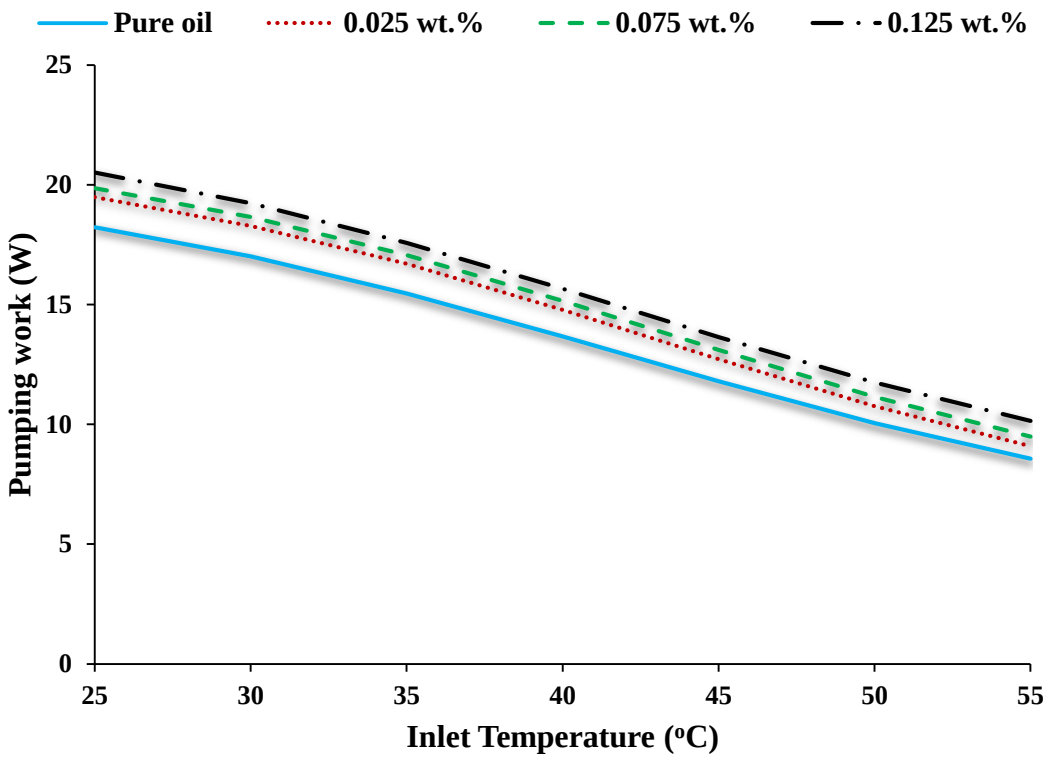

Figure 10. Pumping work demand of the cubical receiver for different inlet temperatures for the examined working fluids.

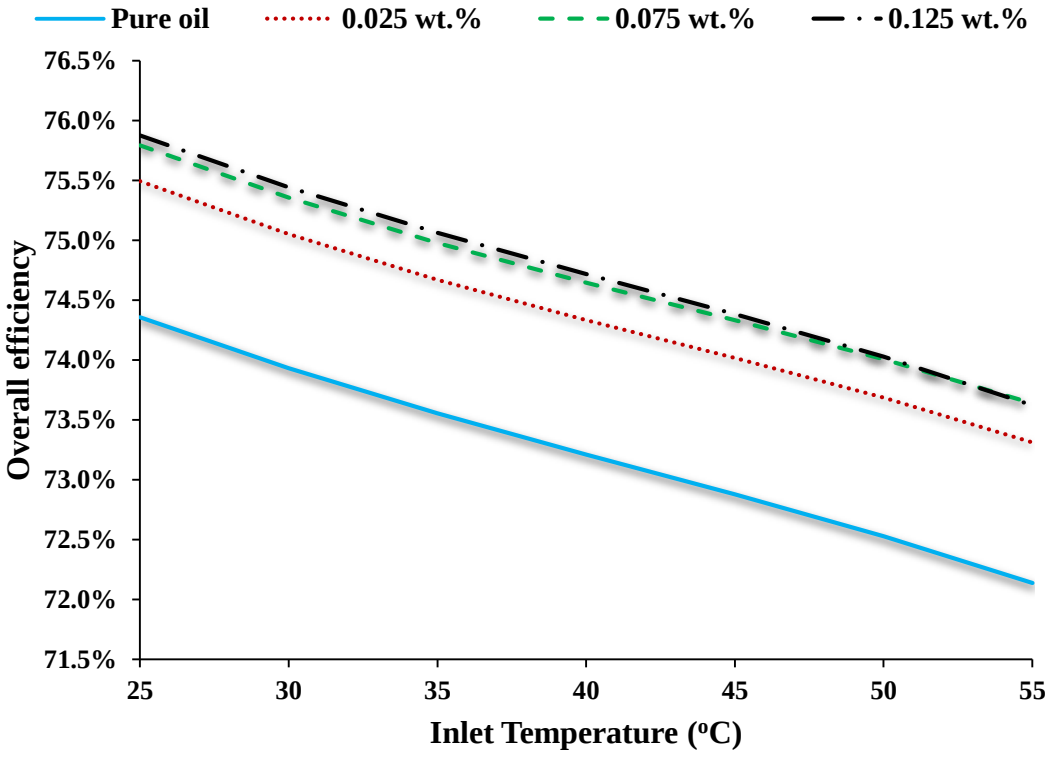

Figure 11. Overall efficiency of the cubical receiver for different inlet temperatures for the examined nanofluids.

3.1.2 Analysis with the cylindrical receiver

This section expresses acquired results for the performance with the cylindrical cavity receiver. Figure 12 shows that higher temperatures reduce the efficiency while higher nanoparticle concentration leads to higher thermal efficiency. These results are similar to the results obtained by the cubical receiver. However, the difference lies in the thermal efficiency enhancements according to Figure 12. More specifically, Figure 13 indicates that the thermal efficiency enhancement is around 1.5%, 1.95%, and 2.1% for the 0.025, 0.075, and 0.125 wt.% concentrations, respectively.

Afterwards, Figure 14 exhibits that the pumping work in the cylindrical cavity is increased with the use of nanofluids. Moreover, higher nanofluid concentration leads to more work demand, which is a reasonable result due to the increased viscosity. Therefore, Figure 15, evaluates the pumping work demand increment through the overall efficiency index. This index showed that the nanofluid utilization was beneficial in the cylindrical cavity. Generally, the use of the 0.125 wt.% concentration is the next one (up to 50^{o}C), while for 55^{o}C the 0.075 wt.% has a minimal increase compared to the 0.125 wt.% case. This result is acceptable due to the higher pumping work seen in the case of the 0.125 wt.% concentration.

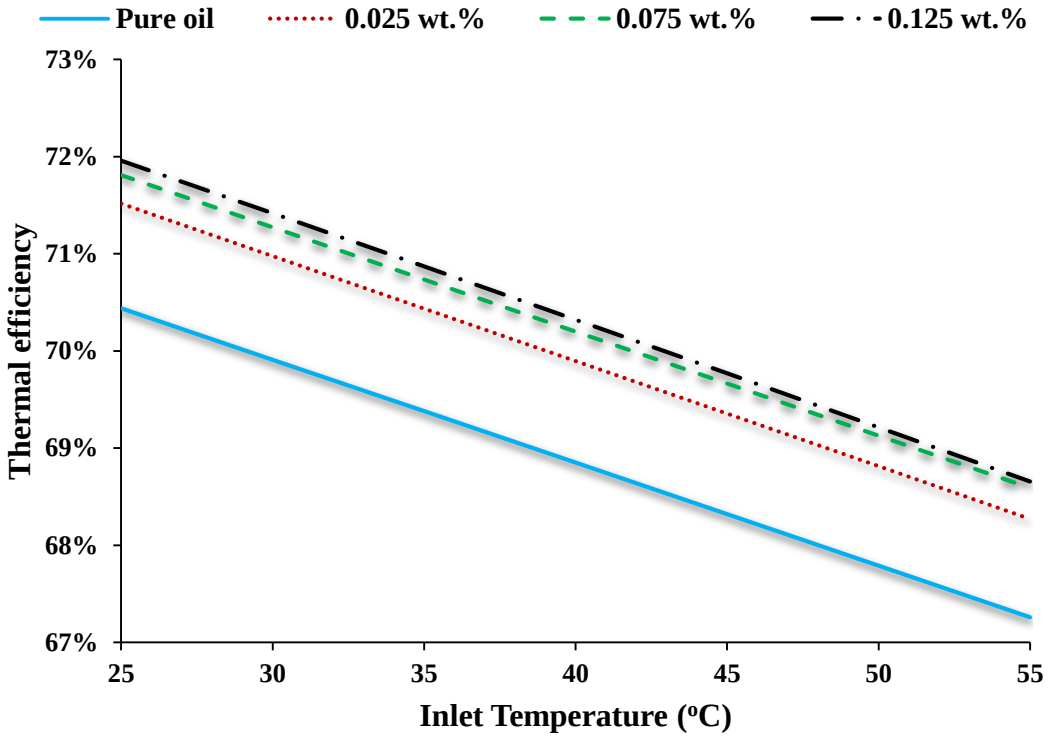

Figure 12. Thermal efficiency of the cylindrical receiver for different inlet temperatures for the examined working fluids.

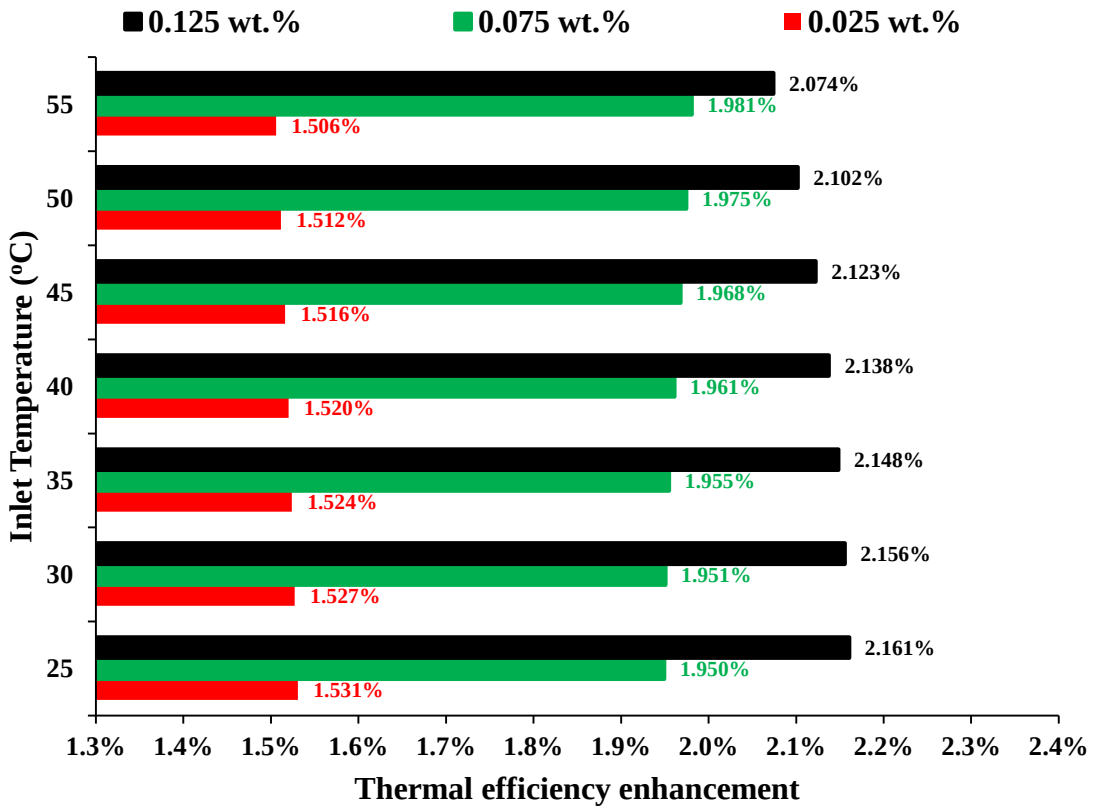

Figure 13. Thermal efficiency enhancement of the cylindrical receiver for different inlet temperatures for the examined nanofluids.

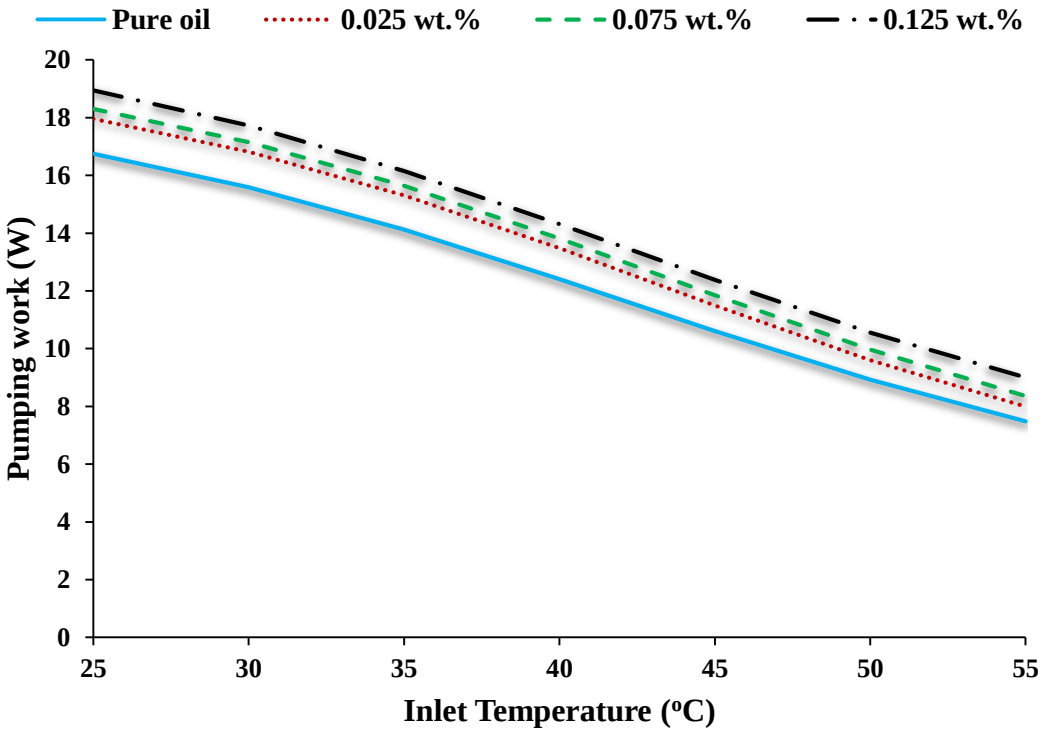

Figure 14. Pumping work demand of the cylindrical receiver for different inlet temperatures for the examined working fluids.

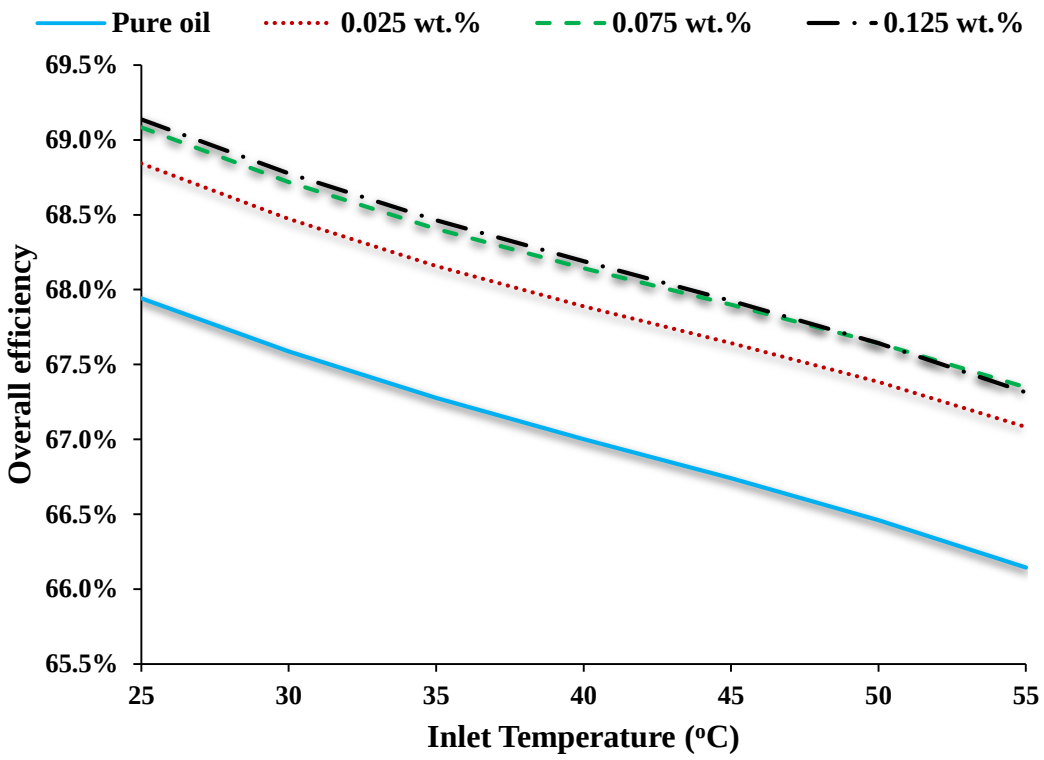

Figure 15. Overall efficiency of the cylindrical receiver for different inlet temperatures for the examined working fluids.

3.1.3 Analysis with the hemispherical receiver

The use of nanofluids in the hemispherical cavity receiver for various temperature levels is examined in this section. Figure 16, exhibits the collector thermal efficiency for the four examined nanofluids. It is obvious that higher nanoparticle concentration leads to higher thermal efficiency, which is a reasonable result that is in accordance with those for other cavities. Figure 17, indicates that the enhancement for the 0.025 wt.% concentration is about 0.4%, while it is 0.5% and 0.55% for 0.075 wt.% and 0.0125 wt.% concentrations, respectively. For the hemispherical cavity, higher operating temperature leads to higher enhancement but at a weak correlation.

The pumping work variation with the temperature is depicted in Figure 18; it is obvious that the concentration increment leads to higher work demand. Another interesting result seen is the higher inlet temperature causing a lower pumping work demand, which is explained by the varying fluid thermal properties. Figure 19, evaluates the pumping work increment through the overall efficiency, whereby it is found that the nanofluids are more beneficial than the pure oil in all cases. The best candidate was the nanofluid at 0.125 wt.% concentration for all inlet temperatures examined. Lastly, it must be noted that the overall efficiency decrement along with the increased inlet temperature are reasonable and associated with the decreased thermal efficiency. In practice, the overall efficiency follows the thermal efficiency and takes up slightly lower values in consideration of the pumping work demand.

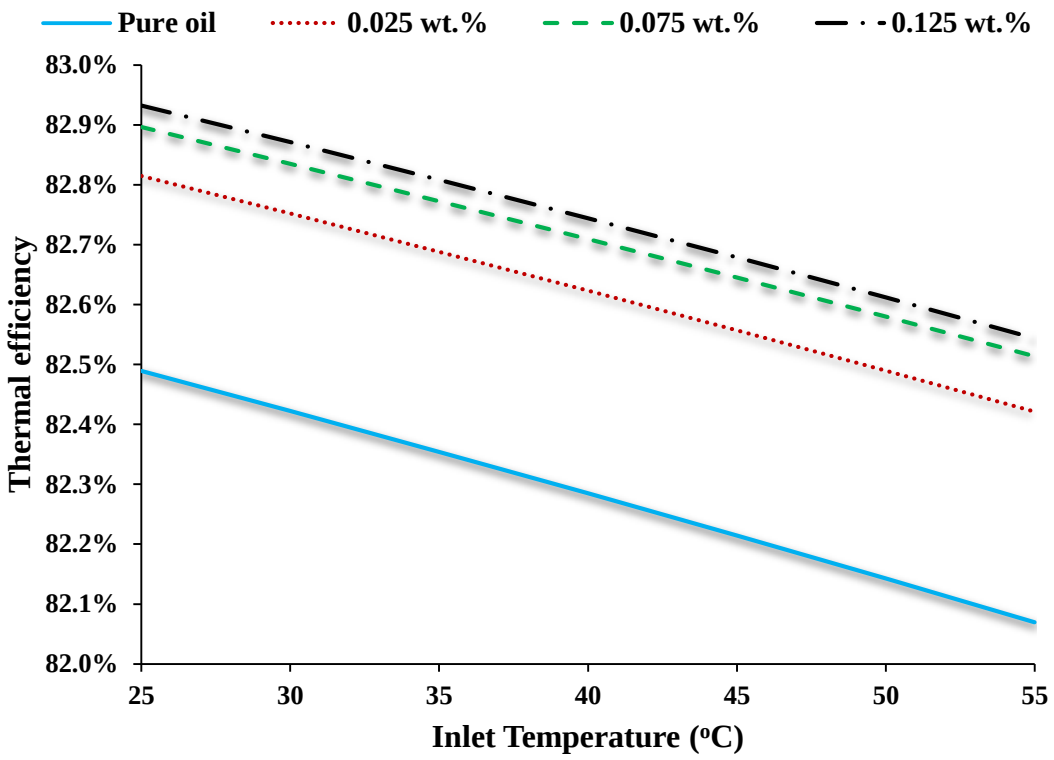

Figure 16. Thermal efficiency of the hemispherical receiver for different inlet temperatures for the examined working fluids.

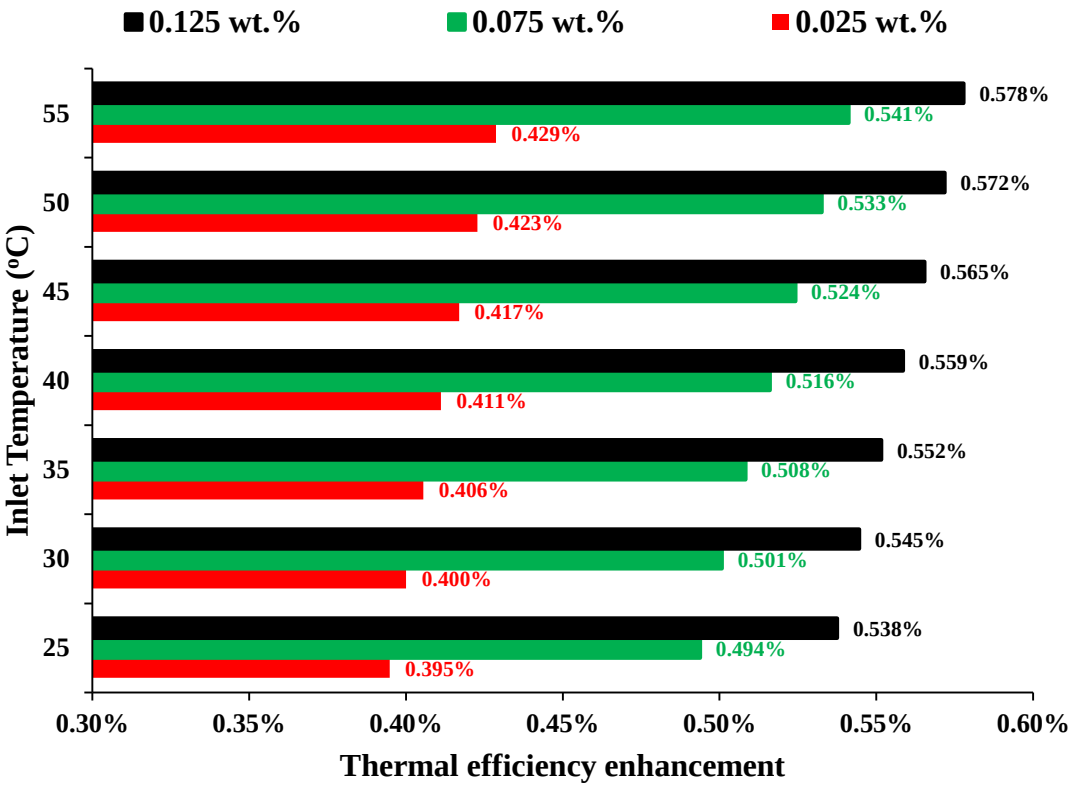

Figure 17. Thermal efficiency enhancement of the hemispherical receiver for different inlet temperatures for the examined nanofluids.

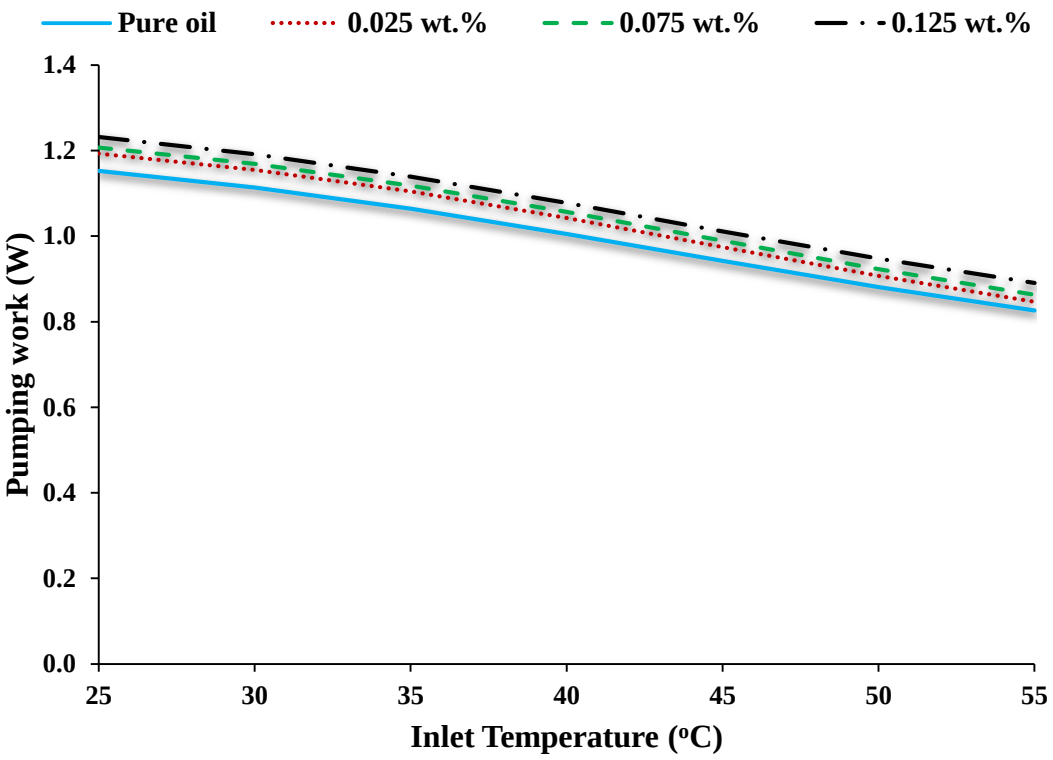

Figure 18. Pumping work demand of the hemispherical receiver for different inlet temperatures for the examined working fluids.

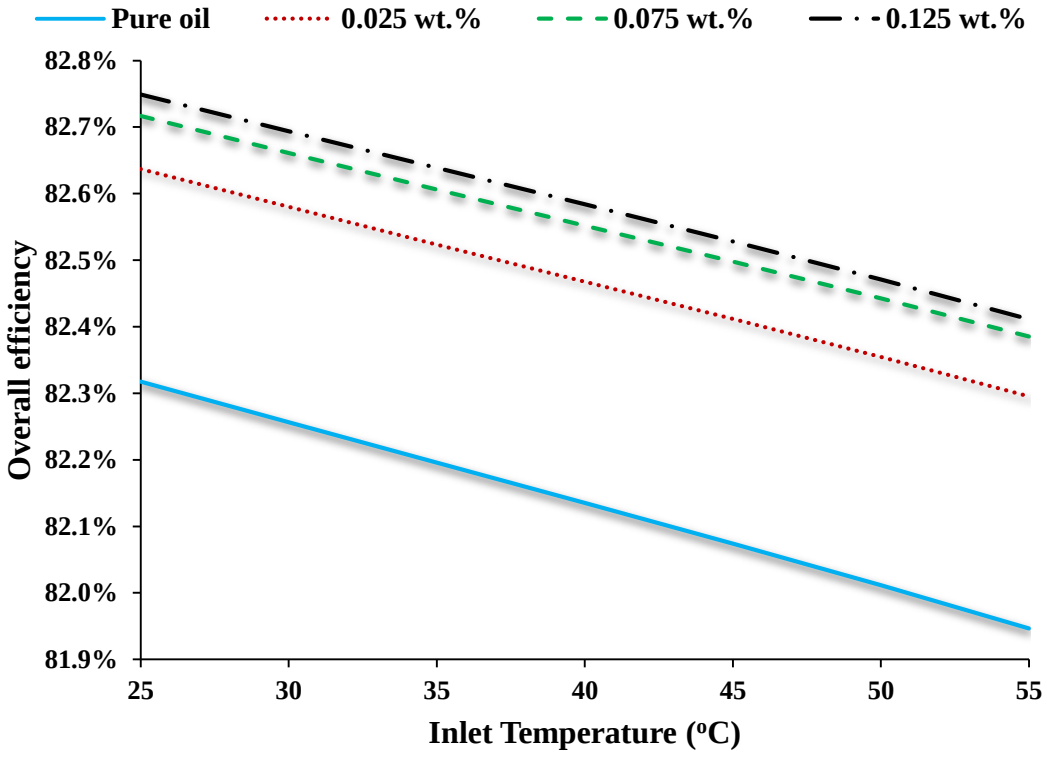

Figure 19. Overall efficiency of the hemispherical receiver for different inlet temperatures for the examined working fluids.

3.1.4 Comparison of the different cavity receivers

Section 3.1.4 summarizes the results for the three cavities and comparison is conducted according to the different inlet temperatures. The results of the best nanofluid candidate (i.e. 0.125 wt.% concentration) are presented and compared with the respective results obtained using pure thermal oil.

Figure 20, depicts the thermal efficiency and thermal efficiency enhancement for the three types of cavities. The hemispherical cavity was obviously the best option, followed by cubical and lastly cylindrical as the least efficient choice. The hemispherical cavity and the cubical cavity have generally more compact shapes, thus resulting in lower thermal losses and rendering them as the most efficient choices. In contrast, the thermal efficiency enhancement in the hemispherical cavity was smaller in comparison with other cavities. This result is reasonable as higher thermal efficiency of the hemispherical cavity leads to a lower margin for thermal enhancement with the use of nanofluids. Therefore, cubical and cylindrical cavities led to enhancements of over 2%, while the hemispherical cavity yielded enhancement up to 0.5% using the examined conditions.

Figure 21, shows the pumping work demand and its increase compared to the base fluid case. The pumping work was significantly lower for the hemispherical cavity as this design had a lower tube length, resulting in lower pressure losses. Moreover, the increment of nanofluid was lower in this design compared to others. At this point, it should be said that the pumping work is up to 21 W, while the useful heat production is up to 1.6 kW approximately. This fact positions the huge difference between these values, thus proving that the pumping work is not a limitation and problem for the examined collector. Therefore, the use of nanofluids is associated with higher pressure drop, which is not an impactful problem as it is also validated by the results of Figure 22. The overall efficiency is given in Figure 22, whereby the use of nanofluids leads to improvement in all the cases. The hemispherical cavity presented the maximum overall efficiency but the lowest enhancement. Similar results were found for thermal efficiency, which is reasonable as these efficiencies are associated with each other.

Finally, the hemispherical cavity design is the most effective choice for the application in dish collectors. Both thermal efficiency and overall efficiency indicated its propriety, as well as the minimum pumping work demand required as calculated in this study. So, this design will be used in the following sections for a deeper investigation.

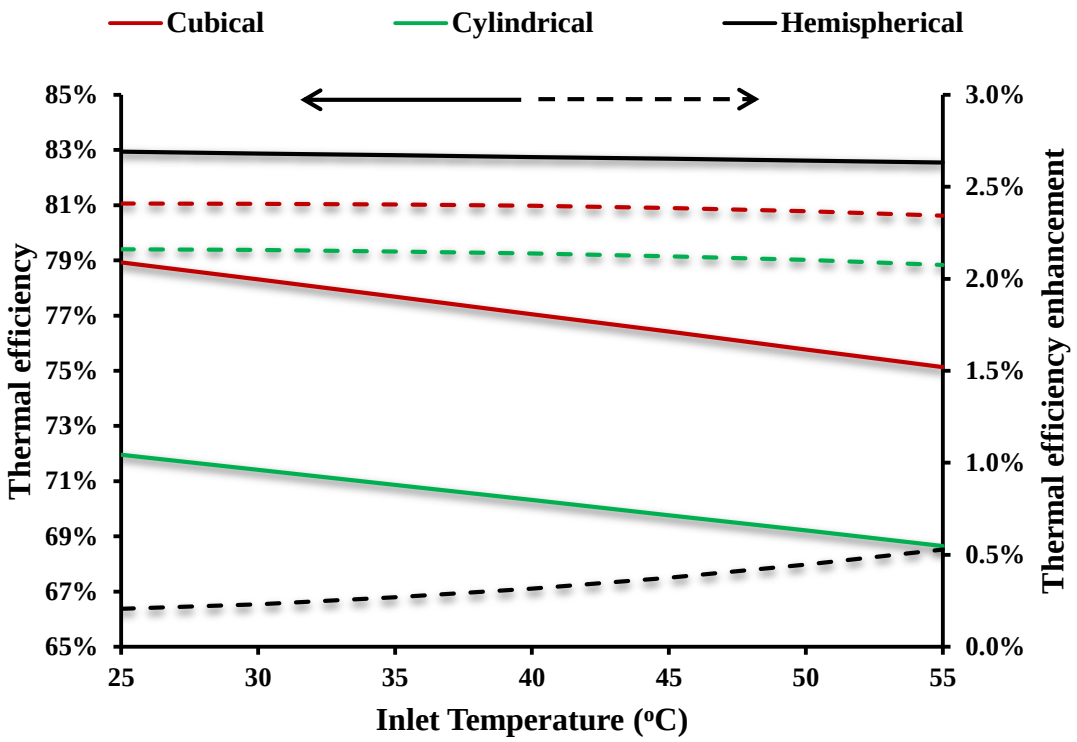

Figure 20. Thermal efficiency of the three cavities with the nanofluid of 0.125 wt.% and enhancement compared to pure oil case.

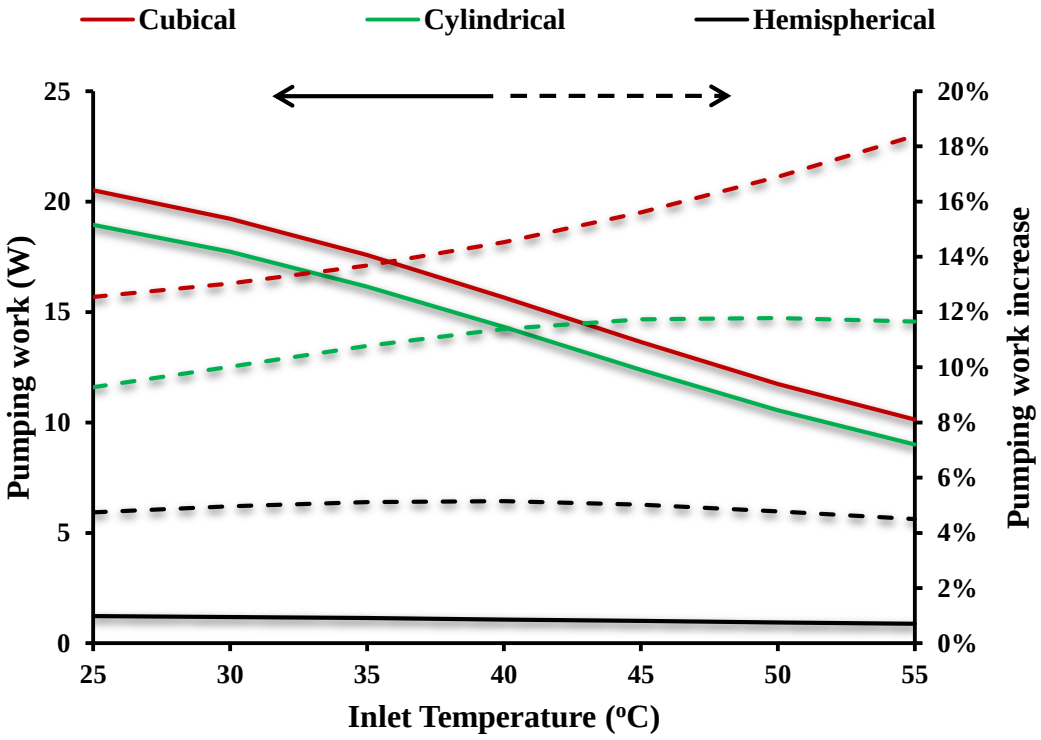

Figure 21. Pumping work of the three cavities with the nanofluid of 0.125 wt.% and increase compared to pure oil case.

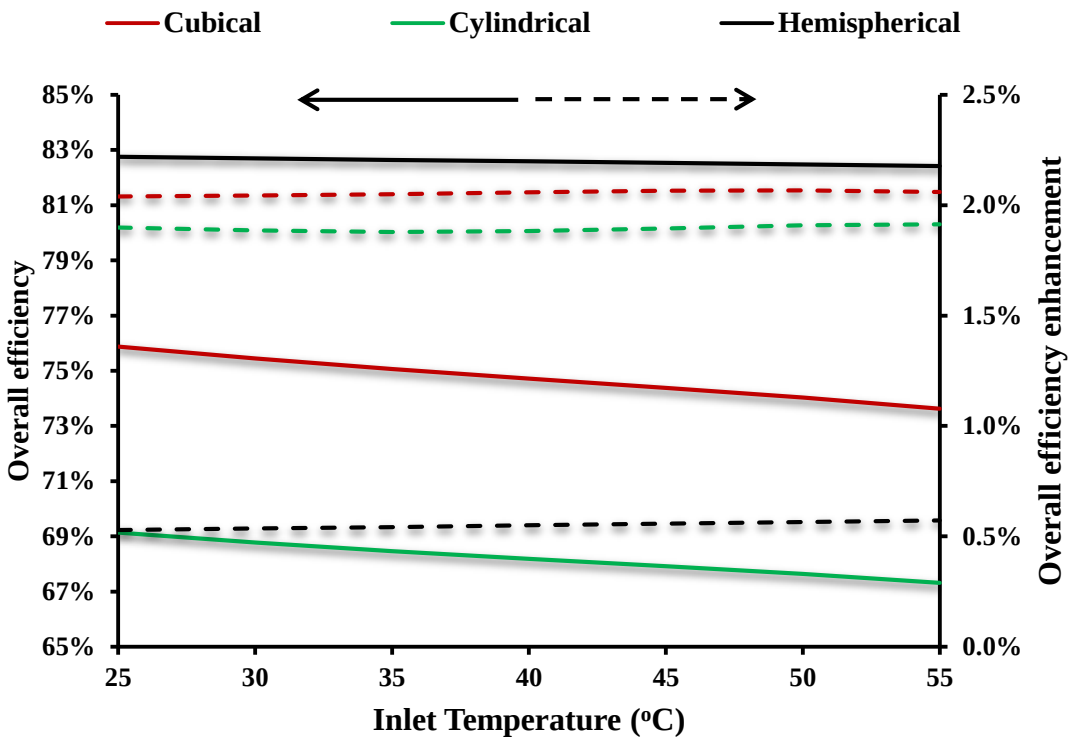

Figure 22. Overall efficiency of the three cavities with the nanofluid of 0.125 wt.% and enhancement compared to pure oil case.

3.2 Parametric analysis of hemispherical cavity

Section 3.2 is devoted to present the results of parametric performance by the hemispherical cavity receiver with nanofluid (i.e. 0.125 wt.%) and pure thermal oil. Different volumetric flow rates and solar beam irradiation levels are examined and, in every case, only one parameter changes.

3.2.1 The impact of the volumetric flow rate on the results

The impact of the volumetric flow rate on the results is examined in section 3.2.1. The inlet temperature was kept constant at 35°C and the solar irradiation was fixed as 800 W/m^2, while the flow rate ranged from 5 up to 150 ml/s.

Figure 23, demonstrates the thermal efficiency and thermal efficient enhancement for different flow rates using the hemispherical design. The higher flow rates increased the thermal efficiency and reduced thermal efficiency enhancement, which is reasonable due to higher flow rates generating higher efficiency. Consequently, smaller enhancement margin is obtained. In practice, flow rates over 50 ml/s required the collector to have a relatively high efficiency. So, the initial selection of the 100 ml/s as the default flow rate is justified.

Figure 24, depicts the results of the pumping work demand. It is obvious that higher volumetric flow rates lead to a significant increase in the pumping work demand. This is a reasonable result due to the direct correlation between these parameters. In practice, the pressure drop depended on the second power of the flow rate and consequently, the

pumping work relied on the second power of flow rate. The shape of the curves in Figure 25 validates this argument. For a small flow rate of 5 ml/s, a huge increase in the pumping work as a percentage (~73%) was obtained. This result seems to be important; however, the extremely low values (~0.01 W) of the work demand in this flow rate make this increment meaningless. In higher flow rates, the increase of the work demand with nanofluid compared to the pure oil is reduced, which is generally around 10%.

Figure 25, shows the impact of the flow rate to the overall efficiency. Higher flow rate increases the thermal efficiency (Figure 23) and pumping work (Figure 24), simultaneously. These results lead to the development of an optimum region of flow rates in the range of 25 to 100 ml/s. This is an interesting result as it indicates the importance of the calculation of the overall efficiency to be used for sizing the system flow rate. In any case, the variation of the overall efficiency is not huge; a small difference in the selected flow rate does not significantly impact on the collector behaviour. The overall efficiency enhancement with the use of nanofluid is similar to that found in thermal efficiency. However, a rough decrement is seen in the enhancement of the overall efficiency due to the incorporation of the pumping work on the analysis.

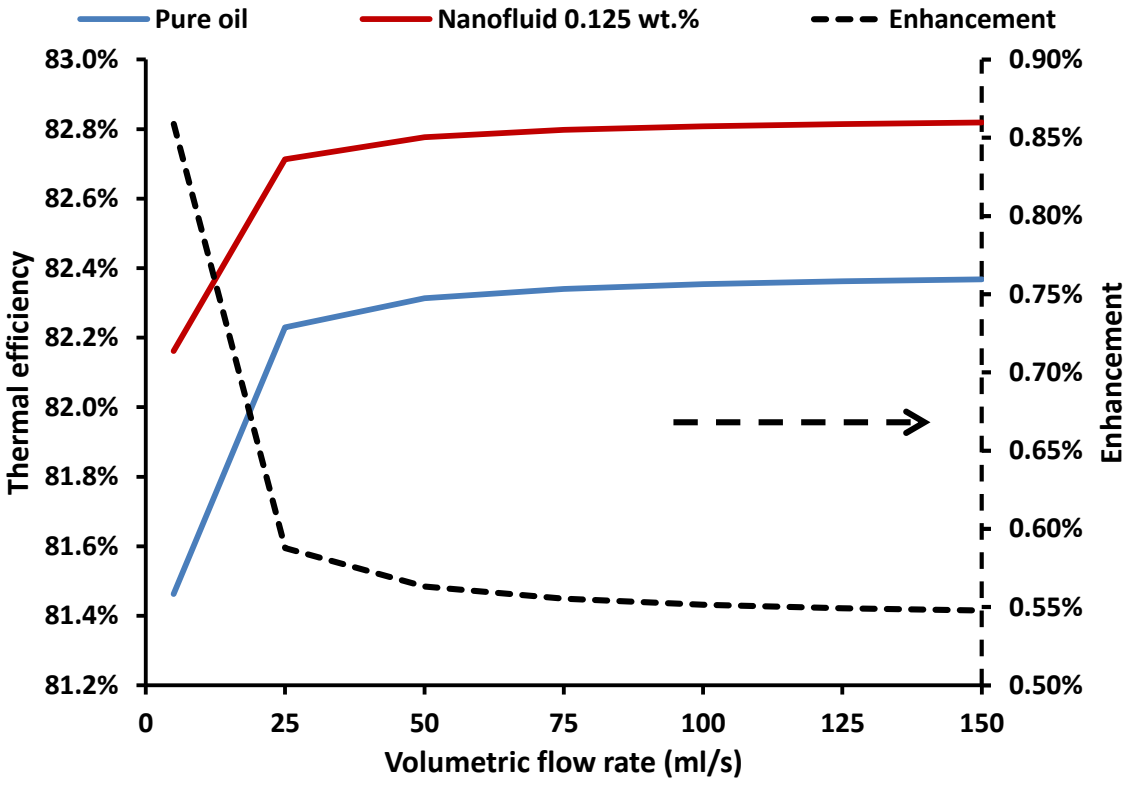

Figure 23. Thermal efficiency of the hemispherical nanofluid 0.125 wt.% for different volumetric flow rates and enhancement compared to the pure oil case.

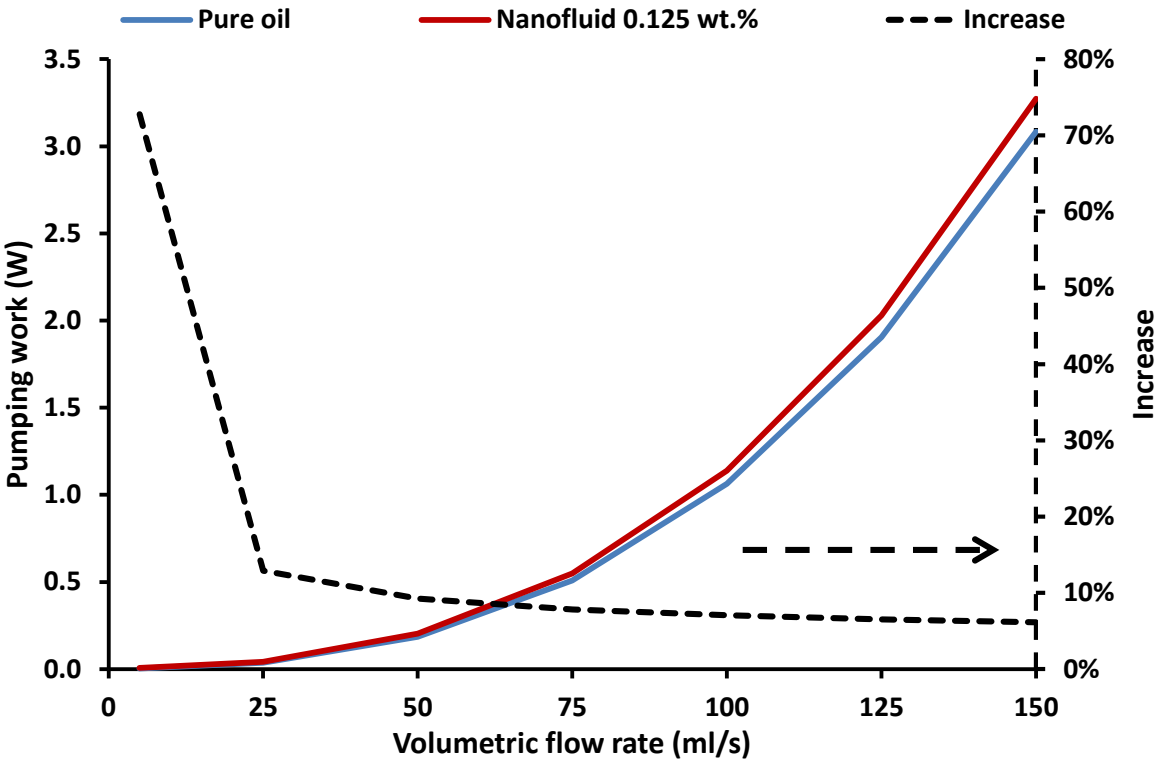

Figure 24. Pumping work of the hemispherical nanofluid 0.125 wt.% for different volumetric flow rates and increase compared to the pure oil case.

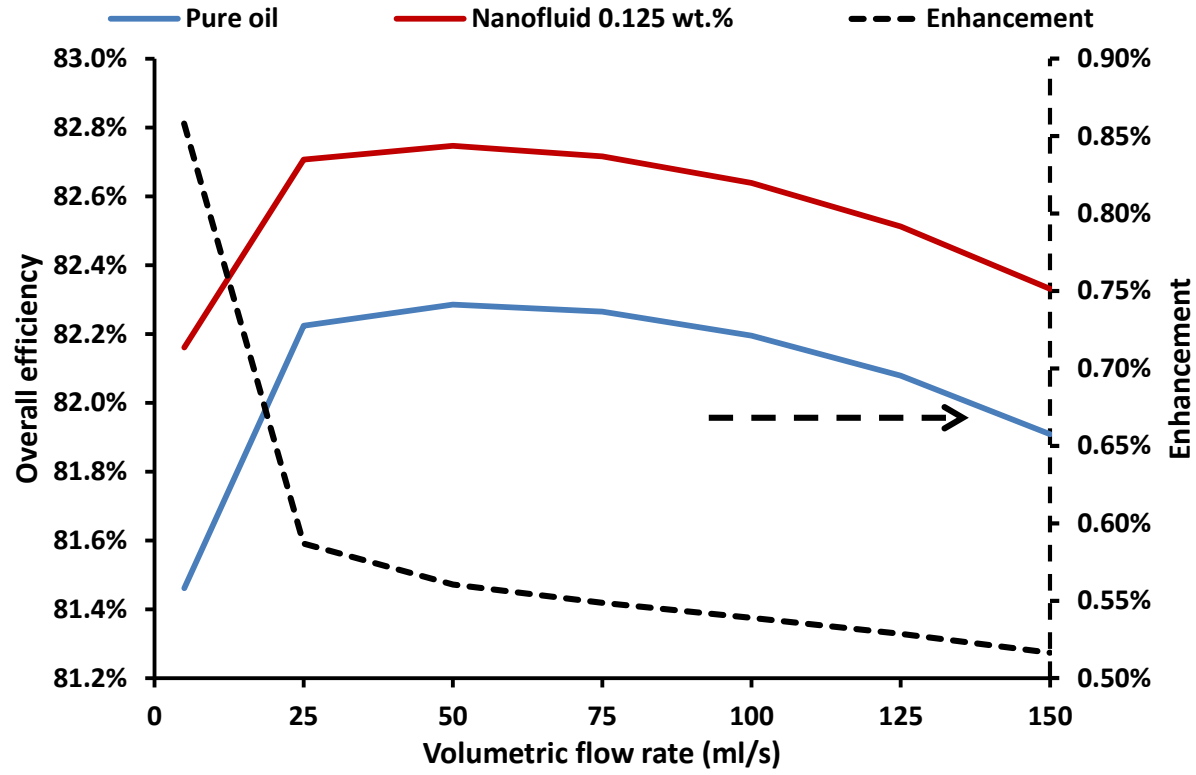

Figure 25. Overall efficiency of the hemispherical nanofluid 0.125 wt.% for different volumetric flow rates and enhancement compared to the pure oil case.

3.2.2 The impact of the solar irradiation on the results

The impact of the solar irradiation level is investigated for the hemispherical cavity in section 3.2.2. The solar beam irradiation is studied ranging from 600 up to 900 W/m^2, which is a reasonable operating range for sunny days. The inlet temperature was kept constant at 35^{o}C and the flow rate at 100 ml/s. In this section, the impact of the solar irradiation on thermal and overall efficiencies is given accordingly. In contrast, the impact of the solar irradiation on the pumping work is not presented as it is found to be negligible.

Figure 26, illustrates the thermal efficiency and thermal efficiency enhancement for the different values of the solar beam irradiation levels. Higher solar irradiation levels lead to higher thermal efficiency, as well as an increased thermal efficiency enhancement. Similarly, higher solar irradiation leads to higher available amounts of solar energy per absorber area, rendering the possibility for higher heat production. Moreover, the higher heat might cause the collector to manage the thermal enhancement with the nanofluid; thus, the enhancement is also improved with the solar irradiation level. Generally, the enhancement is found to be approximately 0.56%. Figure 27 exhibits the overall efficiency and overall efficiency enhancement for the different values of the solar beam irradiation levels. Higher solar irradiation levels lead to the higher overall efficiency and an increase in the respective enhancement is seen. The results obtained are similar to the irradiation impact on the thermal efficiency but with a slightly lower values of the overall efficiency.

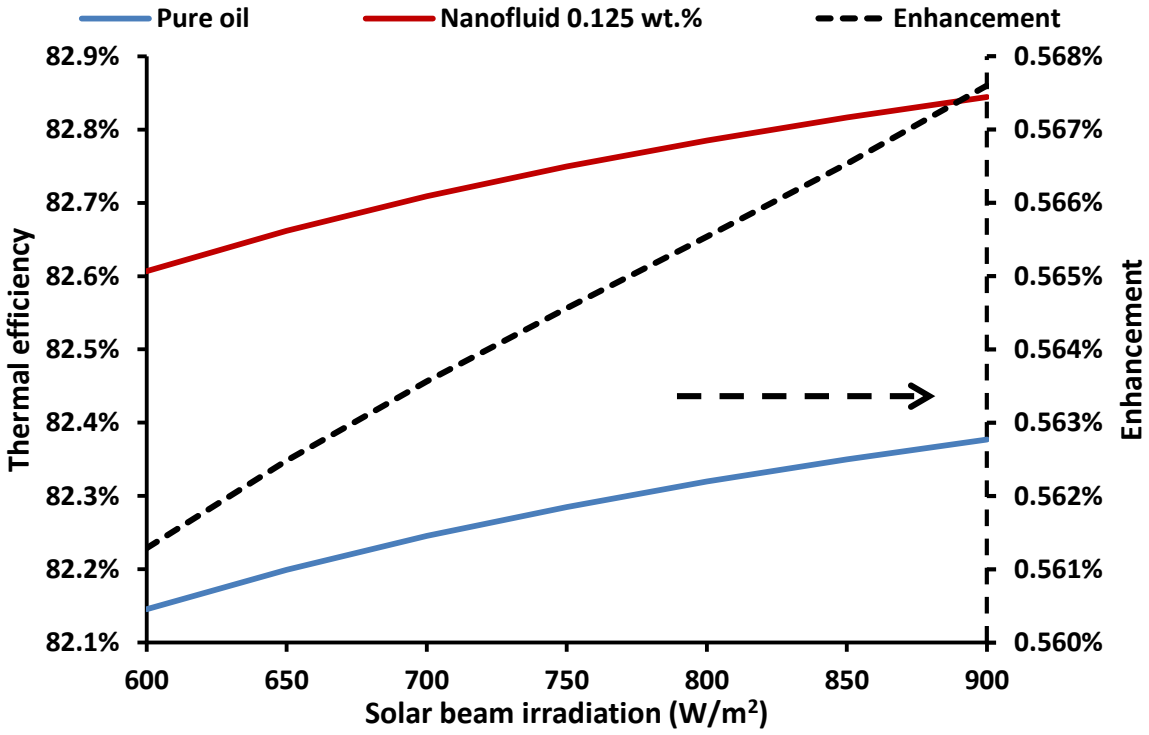

Figure 26. Thermal efficiency of the hemispherical nanofluid 0.125 wt.% for different solar beam irradiation values and enhancement compared to the pure oil case.

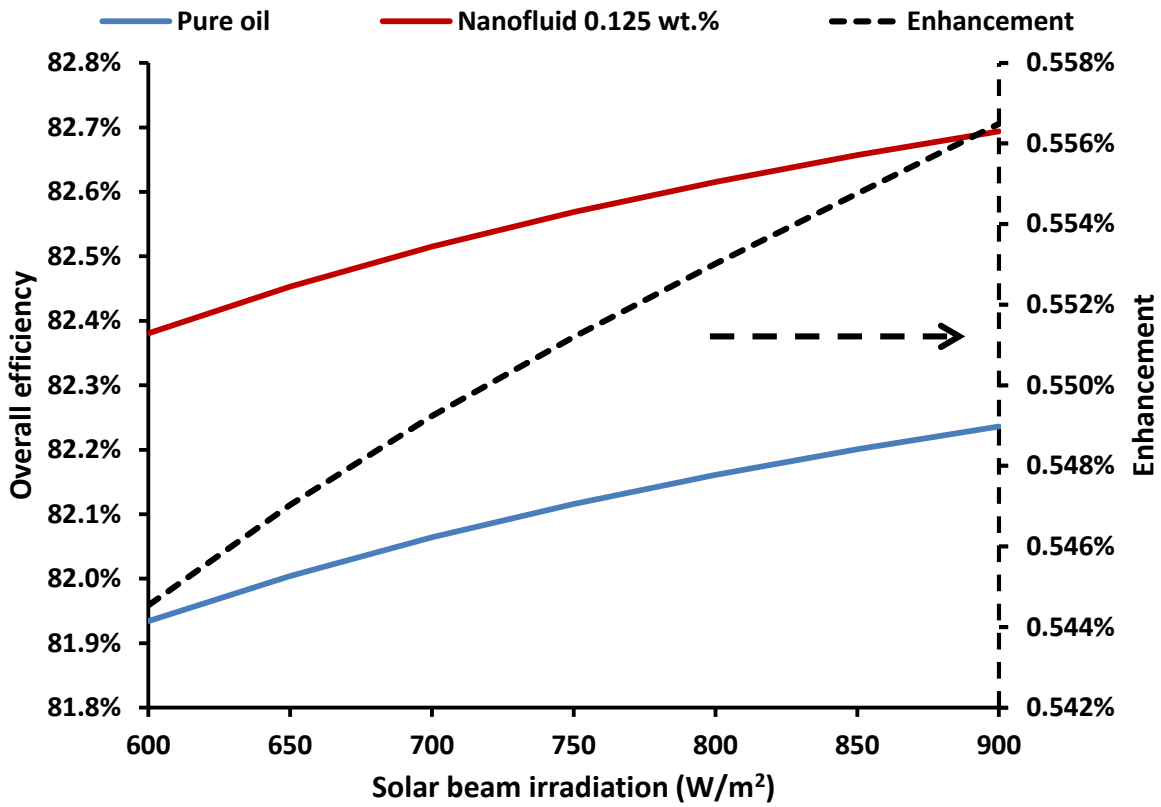

Figure 27. Overall efficiency of the hemispherical nanofluid 0.125 wt.% for different solar beam irradiation values and enhancement compared to the pure oil case.

3.2.3 Daily performance of the system

The next step in this work is associated with the evaluation of the hemispherical cavity receiver with nanofluid at 0.125 wt.% concentration and pure oil on daily basis. Real weather data for a sunny day in Tehran, Iran were used, and the system performance was calculated in the selected day from 9:00 up to 15:30. Figure 28, shows the variation of the thermal and overall efficiencies for nanofluid and pure oil cases. It is obvious that during daytime, the nanofluid leads to higher efficiency in thermal and overall terms. The thermal efficiency is found to be a bit higher than the overall efficiency.

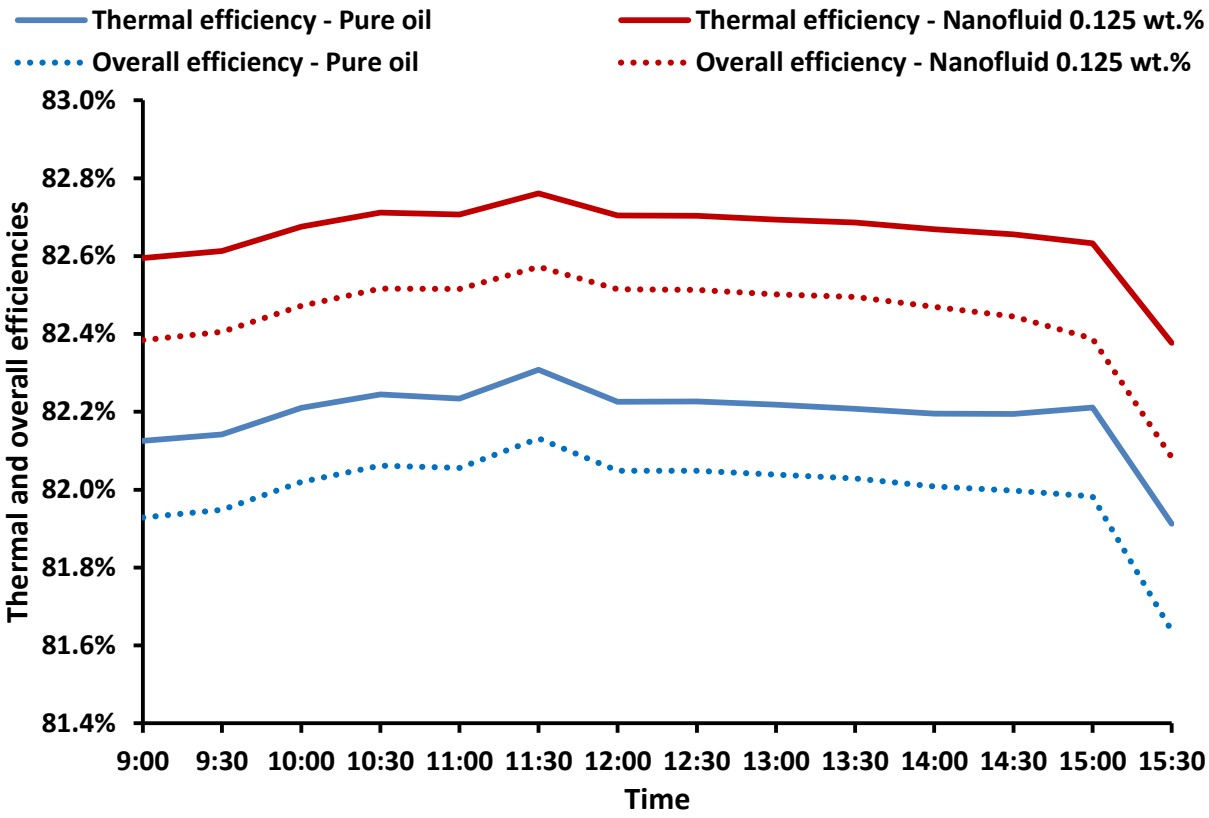

Figure 28. Daily variation of the thermal and overall efficiencies with nanofluid 0.125 wt.% and the respective enhancement compared to the pure oil case.

Table 3, expresses the daily results of the pure oil case while Table 4 gives the results for the nanofluid case, which also include the weather data used. An interesting result noted is that the outlet temperature is lower with the nanofluid in comparison with pure oil, while the efficiencies are higher with the nanofluid. This result is described by the increased specific heat capacity of the nanofluid as seen in Figure 4. In practice, the increased specific heat capacity and density of the nanofluid lead to a higher capacity for storing energy, while the higher thermal conductivity leads to better heat transfer rates inside the flow. So, the mean operating temperature of the absorber is reduced, which leads to lower thermal losses and consequently a higher efficiency with nanofluids.

Lastly, Table 5 expresses the results for the daily collector performance with the two main working fluids. The mean daily thermal efficiency enhancement was 0.57% with the use of nanofluid, while the mean daily overall efficiency enhancement was 0.55%. Next, the mean increase in the pumping work was 7.06%, while the mean outlet temperature decrease was 3.55% or 1.56 K.

Table 3. Daily results for the collector performance with pure oil (V =100 ml/s – T_{in} =35˚C)

Time (h)	T_{amb} (˚C)	V_w (m/s)	I_b (W/m^2)	T_{out} (˚C)	Q_u (W)	η_{th} (%)	W (W)	η_{ovr} (%)
9:00	20.6	3.2	643	43.94	1343	82.13	1.064	81.93
9:30	21.9	3.5	654	44.10	1367	82.14	1.064	81.95
10:00	27.3	2.4	666	44.27	1393	82.21	1.064	82.02
10:30	29.4	2.6	695	44.67	1454	82.24	1.064	82.06
11:00	28.0	3.5	711	44.90	1487	82.23	1.064	82.06
11:30	29.1	1.2	719	45.02	1506	82.31	1.064	82.13
12:00	29.0	5.2	715	44.95	1495	82.23	1.064	82.05
12:30	28.6	4.6	713	44.92	1490	82.23	1.064	82.05
13:00	27.6	4.3	706	44.83	1477	82.22	1.064	82.04
13:30	27.1	5.3	708	44.86	1481	82.21	1.064	82.03
14:00	27.1	4.0	680	44.46	1421	82.20	1.064	82.01
14:30	27.0	2.0	642	43.93	1342	82.19	1.064	82.00
15:00	27.0	0.2	556	42.74	1163	82.21	1.064	81.98
15:30	26.9	3.3	463	41.42	965	81.91	1.064	81.64

Table 4. Daily results for the collector performance with nanofluid 0.125 wt.% (V =100 ml/s – T_{in} =35˚C)

Time (h)	T_{amb} (˚C)	V_w (m/s)	I_b (W/m^2)	T_{out} (˚C)	Q_u (W)	η_{th} (%)	W (W)	η_{ovr} (%)
9:00	20.6	3.2	643	42.42	1351	82.59	1.139	82.38
9:30	21.9	3.5	654	42.55	1375	82.61	1.139	82.41
10:00	27.3	2.4	666	42.69	1401	82.68	1.139	82.47
10:30	29.4	2.6	695	43.03	1462	82.71	1.139	82.52
11:00	28.0	3.5	711	43.21	1496	82.71	1.139	82.52
11:30	29.1	1.2	719	43.31	1514	82.76	1.139	82.57
12:00	29.0	5.2	715	43.26	1504	82.70	1.139	82.51
12:30	28.6	4.6	713	43.23	1499	82.70	1.139	82.51
13:00	27.6	4.3	706	43.16	1485	82.69	1.139	82.50
13:30	27.1	5.3	708	43.18	1490	82.69	1.139	82.49
14:00	27.1	4.0	680	42.85	1429	82.67	1.139	82.47
14:30	27.0	2.0	642	42.41	1350	82.66	1.139	82.44
15:00	27.0	0.2	556	41.42	1169	82.63	1.139	82.39
15:30	26.9	3.3	463	40.33	970	82.38	1.139	82.08

Table 5. Final comparison of the pure oil and nanofluid on a daily basis (V =100 ml/s – T_{in} =35˚C)

	$T_{out,m}$ (˚C)	E_b (kWh)	E_u (kWh)	E_w (kWh)	η_{th} (%)	η_{ovr} (%)
Pure oil	44.21	10.95	9.00	0.069	82.20	82.01
Nanofluid 0.125 wt.%	42.65	10.95	9.07	0.074	82.66	82.46
Difference (%)	-3.55	-	0.57	7.06	0.57	0.55

3.3 Discussion and future work

This work examines a nanofluid-based solar dish collector. The system is studied in relatively low temperatures due to the available thermal properties of the nanofluid in this range. An important advantage of the examined nanofluid is its increased density and specific heat capacity, while other nanofluids present increased density but at a decreased specific heat capacity. So, the novel soybean oil-based MXene nanofluid is an important candidate for thermal applications. More specifically, the present system can be applied in applications such as space heating, domestic hot water production, solar cooling with adsorption machines, desalination and, generally as an assisting device in a greater system.

In this work, it is found that the use of nanofluids enhances the thermal and overall efficiency of the solar collector. This is a reasonable result, which can also be found in other literature. Furthermore, the increased pumping work is not a problem due to the low values of this parameter. The useful heat production is about 1500 to 1700 W, while the maximum found values of the pumping work is up 21 W. So, it can be said that the limitation of the nanofluid high viscosity is not an obstacle in the present application.

Another interesting result found is the lower thermal efficiency enhancement in the cases with higher efficiency; hence, the thermal efficiency enhancement margin is lower. Therefore, the enhancements in cubical and cylindrical cavities are higher compared to the hemispherical-shaped cavity. However, the hemispherical case is the most efficient and promising design.

In the future, the need for examining the system at higher temperature levels is noted when the available thermal properties for the nanofluid are in higher temperatures. In addition, a detailed study of financial analysis and risk analysis about the nanofluid agglomeration issues is required. Lastly, the present nanofluid can be used in other solar systems, such as flat plate collector, thermal photovoltaic and parabolic trough collector.

4. Conclusions

This work aims to investigate a novel nanofluid (soybean oil-based MXene) in a solar dish collector. Three different cavity receivers are examined, including cylindrical, cubical, and hemispherical shapes. The analysis is conducted using a numerical model, which is developed and validated with experimental results. The

thermal properties of the nanofluid are taken from experimental data and the nanofluid is studied at the concentrations of 0.025 wt.%, 0.075 wt.% and 0.125 wt.%. The important conclusions of this work are summarized as below:

- The hemispherical cavity is the best candidate for all examined working fluids and operating temperatures. Moreover, the nanofluid with the maximum examined concentration of 0.125 wt.% is the best candidate among working fluids.

- The thermal efficiency enhancement with the hemispherical nanofluid is around 0.5%, while other cavities yield 2% to 2.5%. The higher enhancement with the cubical and cylindrical shapes is justified due to the lower efficiency values, which give higher enhancement margins.

- The use of nanofluid leads to a pumping work increment, which is generally around 10%. However, this factor might not eliminate the overall enhancement of the collector. This fact has been tested by investigating the overall efficiency.

- The volumetric flow rate and solar beam irradiation level increments increase the thermal efficiency. The enhancement with the nanofluid is maximized at low volumetric flow rates and high solar irradiation levels.

- The daily efficiency of the solar collector with the nanofluids is 82.66% and it is enhanced by 0.57% compared to pure oil (82.20%). The daily yield of the examined collector is 9.07 kWh.

Nomenclature

A	Area, m^2
c_p	Specific heat capacity, J/kgK
c_2	constant parameter, W/m^2
d	Diameter, m
D	Aperture diameter, m
F	View factor
f_r	Friction factor
h	Cavity height, m
h'	Heat transfer coefficient, W/m^2K
I_b	Solar beam irradiation, W/m^2
k	Thermal conductivity, W/mK
L	Length of tubing, m
$\dot{m}$	Mass flow rate, kg/s
m_2	constant parameter, W/mK
N	Number of segments
Nu	Nusselt number
Pr	Prandtl number
$\dot{Q}_{loss}$	Thermal losses, W
$\dot{Q}_{solar}$	Received solar energy, W
$\dot{Q}_u$	Useful heat production by the collector, W

$\dot{Q}^*$ Absorbed energy rate, W
R Thermal resistance, m^2K/W
Re Reynolds number
T_{in} inlet temperature, °C
T_s Surface temperature, °C
T_{oo} Environment temperature, °C
V Volumetric flow rate, ml/s
V_{wind} Wind speed, m/s
W Pump work demand, W

Greek symbols

ΔP Pressure drop, Pa
ε Emittance
η_{th} Thermal efficiency
η_{conv} Conversion efficiency
η_{ovr} Overall efficiency
σ Stefan-Boltzmann constant (= $5.67 \cdot 10^{-8}$ W/m^2K^4)

Subscripts and Superscripts

amb ambient
ap aperture
cond conduction
conv convection
dish dish concentrator
fluid working fluid
in inlet
inner inner surface
out outlet
rad radiation
n number of element
tube tube
0 at initial

Acknowledgement

Dr. Loni, and Dr. Najafi are grateful to the Tarbiat Modares University (http://www.modares.ac.ir) for financial supports given under IG/39705 grant for renewable Energies of Modares research group. "R. Saidur would like to acknowledge the financial support provided by the Sunway University through the project no# STR-RCTR-RCNMET-001-2019". The author W.S.W. Harun would like to recognize the support of the Fundamental Research Grant Scheme FRGS/1/2019/TK03/UMP/02/15 and K.Kadirgama would like acknowledge Universiti Malaysia Pahang for providing financial assistant under grant No. RDU192209 .

References

1. Abdulhamed, A.J., et al., *Review of solar parabolic-trough collector geometrical and thermal analyses, performance, and applications.* Renewable and Sustainable Energy Reviews, 2018. **91**: p. 822-831.
2. Gorjian, S., et al., *A review on recent advancements in performance enhancement techniques for low-temperature solar collectors.* Energy Conversion and Management, 2020. **222**: p. 113246.
3. Loni, R., et al., *Performance study of a solar-assisted organic Rankine cycle using a dish-mounted rectangular-cavity tubular solar receiver.* Applied Thermal Engineering, 2016. **108**: p. 1298-1309.
4. Reddy, K., et al., *Effect of wind speed and direction on convective heat losses from solar parabolic dish modified cavity receiver.* Solar Energy, 2016. **131**: p. 183-198.
5. Guarino, S., et al., *A dish-stirling solar concentrator coupled to a seasonal thermal energy storage system in the southern mediterranean basin: A cogenerative layout hypothesis.* Energy Conversion and Management, 2020. **222**: p. 113228.
6. Loni, R., et al., *Optimizing the efficiency of a solar receiver with tubular cylindrical cavity for a solar-powered organic Rankine cycle.* Energy, 2016. **112**: p. 1259-1272.
7. Pavlovic, S., et al., *Comparative study of spiral and conical cavity receivers for a solar dish collector.* Energy Conversion and Management, 2018. **178**: p. 111-122.
8. Günther, M., et al., *Solar Dish Technology.* Advanced CSP teaching materials,2011. **1**: p. 1-63.
9. Rafiei, A., et al., *Thermal analysis of a hybrid solar desalination system using various shapes of cavity receiver: cubical, cylindrical, and hemispherical.* Energy Conversion and Management, 2019. **198**: p. 111861.
10. Saidur, R., et al., *A review on applications and challenges of nanofluids.* Renewable and sustainable energy reviews, 2011. **15**(3): p. 1646-1668.
11. Loni, R., et al., *Thermal performance comparison between Al 2 O 3/oil and SiO 2/oil nanofluids in cylindrical cavity receiver based on experimental Study.* Renewable Energy, 2018.
12. Daabo, A.M., et al., *The optical efficiency of three different geometries of a small scale cavity receiver for concentrated solar applications.* Applied Energy, 2016. **179**: p. 1081-1096.
13. Navalho, J.E., et al., *A comprehensive and fully predictive discrete methodology for volumetric solar receivers: application to a functional parabolic dish solar collector system.* Applied Energy, 2020. **267**: p. 114781.
14. Bellos, E., et al., *Optical and thermal analysis of different cavity receiver designs for solar dish concentrators.* Energy Conversion and Management: X, 2019: p. 100013.
15. Venkatachalam, T., et al., *Effect of aspect ratio on thermal performance of cavity receiver for solar parabolic dish concentrator: An experimental study.* Renewable Energy, 2019. **139**: p. 573-581.
16. Loni, R., et al., *Research and review study of solar dish concentrators with different nanofluids and different shapes of cavity receiver: Experimental tests.* Renewable Energy, 2019.

17. Yan, J., et al., *Optimization of a discrete dish concentrator for uniform flux distribution on the cavity receiver of solar concentrator system.* Renewable Energy, 2018.
18. Loni, R., et al., *Numerical comparison of a solar dish concentrator with different cavity receivers and working fluids.* Journal of Cleaner Production, 2018. **198**: p. 1013-1030.
19. Yang, S., et al., *Design and performance evaluation of a high-temperature cavity receiver for a 2-stage dish concentrator.* Solar Energy, 2018. **174**: p. 1126-1132.
20. Soltani, S., et al., *A novel optical-thermal modeling of a parabolic dish collector with a helically baffled cylindrical cavity receiver.* Energy, 2018.
21. Krishna, Y., et al., *State-of-the-art heat transfer fluids for parabolic trough collector.* International Journal of Heat and Mass Transfer, 2020. **152**: p. 119541.
22. Aslfattahi, N., et al., *MXene based new class of silicone oil nanofluids for the performance improvement of concentrated photovoltaic thermal collector.* Solar Energy Materials and Solar Cells, 2020. **211**: p. 110526.
23. Singh, T., et al., *Performance investigation of multiwall carbon nanotubes based water/oil nanofluids for high pressure and high temperature solar thermal technologies for sustainable energy systems.* Energy Conversion and Management, 2020. **225**: p. 113453.
24. Abdelrazik, A., et al., *Optical, stability and energy performance of water-based MXene nanofluids in hybrid PV/thermal solar systems.* Solar Energy, 2020. **204**: p. 32-47.
25. Hong, K., et al., *Numerical simulations of a Cu–water nanofluid-based parabolic-trough solar collector.* Journal of Thermal Analysis and Calorimetry, 2021. **143**(6): p. 4183-4195.
26. Moravej, M., et al., *Enhancing the efficiency of a symmetric flat-plate solar collector via the use of rutile TiO2-water nanofluids.* Sustainable Energy Technologies and Assessments, 2020. **40**: p. 100783.
27. Bozorg, M.V., et al., *CFD study of heat transfer and fluid flow in a parabolic trough solar receiver with internal annular porous structure and synthetic oil–Al2O3 nanofluid.* Renewable Energy, 2020. **145**: p. 2598-2614.
28. Khan, M.S., et al., *Comparative performance assessment of solar dish assisted s-CO2 Brayton cycle using nanofluids.* Applied Thermal Engineering, 2019. **148**: p. 295-306.
29. Pavlović, S.R., et al., *Thermal and exergetic investigation of a solar dish collector operating with mono and hybrid nanofluids.* Thermal Science, 2018. **22**(Suppl. 5): p. 1383-1393.
30. Rajendran, D., et al., *Experimental studies on the thermal performance of a parabolic dish solar receiver with the heat transfer fluids SiC+ water nano fluid and water.* Journal of Thermal Science, 2017. **26**(3): p. 263-272.
31. Loni, R., et al., *Thermal and exergy performance of a nanofluid-based solar dish collector with spiral cavity receiver.* Applied Thermal Engineering, 2018. **135**: p. 206-217.
32. Pavlovic, S., et al., *Exergetic investigation of a solar dish collector with smooth and corrugated spiral absorber operating with various nanofluids.* Journal of Cleaner Production, 2018. **174**: p. 1147-1160.

33. Loni, R., et al., *GMDH modeling and experimental investigation of thermal performance enhancement of hemispherical cavity receiver using MWCNT/oil nanofluid.* Solar Energy, 2018. **171**: p. 790-803.
34. Naguib, M., et al., *Two- dimensional nanocrystals produced by exfoliation of Ti3AlC2.* Advanced Materials, 2011. **23**(37): p. 4248-4253.
35. Aslfattahi, N., et al., *Experimental investigation of energy storage properties and thermal conductivity of a novel organic phase change material/MXene as A new class of nanocomposites.* Journal of Energy Storage, 2020. **27**: p. 101115.
36. Sun, D., et al., *Two-dimensional Ti3C2 as anode material for Li-ion batteries.* Electrochemistry communications, 2014. **47**: p. 80-83.
37. Hu, Q., et al., *MXene: a new family of promising hydrogen storage medium.* The Journal of Physical Chemistry A, 2013. **117**(51): p. 14253-14260.
38. Li, R., et al., *MXene Ti3C2: an effective 2D light-to-heat conversion material.* ACS nano, 2017. **11**(4): p. 3752-3759.
39. Fu, H.C., et al., *MXene- Contacted Silicon Solar Cells with 11.5% Efficiency.* Advanced Energy Materials, 2019. **9**(22): p. 1900180.
40. Guo, Z., et al., *High electrical conductivity 2D MXene serves as additive of perovskite for efficient solar cells.* Small, 2018. **14**(47): p. 1802738.
41. R. Loni, E.A.A.-A., B. Ghobadian, A. Kasaeian, *Experimental study of carbon nano tube/oil nanofluid in dish concentrator using a cylindrical cavity receiver: Outdoor tests.* Energy Conversion and Management, 2018. **165**: p. 593-601.
42. Loni, R., et al., *Numerical and experimental investigation of wind effect on a hemispherical cavity receiver.* Applied Thermal Engineering, 2017. **126**: p. 179-193.
43. Loni, R., et al., *GMDH modeling and experimental investigation of thermal performance enhancement of hemispherical cavity receiver using MWCNT/oil nanofluid.* Solar Energy, 2018. **171**: p. 790-803.
44. Loni, R., et al., *Energy and exergy investigation of alumina/oil and silica/oil nanofluids in hemispherical cavity receiver: Experimental Study.* Energy, 2018. **164**: p. 275-287.
45. Loni, R., et al., *Experimental and Numerical Study on Dish Concentrator with Cubical and Cylindrical Cavity Receivers using Thermal Oil.* Energy, 2018.
46. Le Roux, W.G., et al., *The efficiency of an open-cavity tubular solar receiver for a small-scale solar thermal Brayton cycle.* Energy Conversion and Management, 2014. **84**: p. 457-470.
47. Pavlovic, S., et al., *Exergetic investigation of a solar dish collector with smooth and corrugated spiral absorber operating with various nanofluids.* Journal of cleaner production, 2018. **174**: p. 1147-1160.
48. Cengel, Y.A., et al., *Heat and mass transfer: fundamentals & applications*. Vol. 4. 2011: McGraw-Hill New York.
49. Mwesigye, A., et al., *Thermodynamic optimisation of the performance of a parabolic trough receiver using synthetic oil–Al2O3 nanofluid.* Applied Energy, 2015. **156**: p. 398-412.
50. Rubbi, F., et al., *Performance optimization of a hybrid PV/T solar system using Soybean oil/MXene nanofluids as A new class of heat transfer fluids.* Solar Energy, 2020. **208**: p. 124-138.

Credit Author Statement

All authors contributed according to authorship criteria and guidelines